Foreland Magmatism during the Arabia–Eurasia Collision: Pliocene–Quaternary Activity of the Karacadağ Volcanic Complex, SW Turkey

TANER EKICI[1]*, COLIN G. MACPHERSON[2], NAZMI OTLU[1] AND DENIS FONTIGNIE[3]

[1]DEPARTMENT OF GEOLOGICAL ENGINEERING, UNIVERSITY OF CUMHURIYET, 58140, SIVAS, TURKEY
[2]DEPARTMENT OF EARTH SCIENCES, UNIVERSITY OF DURHAM, DURHAM DH1 3LE, UK
[3]DEPARTMENT OF MINERALOGY, UNIVERSITY OF GENEVA, CH-1205 GENEVA, SWITZERLAND

RECEIVED AUGUST 21, 2013; ACCEPTED JUNE 20, 2014

Pliocene to Quaternary magmatism in the Karacadağ Volcanic Complex in SE Turkey occurred in the foreland region of the Arabia–Eurasia collision and can be divided into two phases. The earlier Karacadağ phase formed a north–south-trending volcanic ridge that erupted three groups of lavas. The same range of mantle sources contributed to the younger Ovabağ phase lavas, which were erupted from monogenetic cones to the east of the Karacadağ fissure. As at several other intraplate localities across the northern Arabian Plate this magmatism represents mixtures of melt from shallow, isotopically enriched mantle and from deeper, more depleted mantle. The deep source is similar to the depleted mantle invoked for other northern Arabian intraplate volcanic fields but at Karacadağ this source contained phlogopite. This source could be located in the shallow convecting mantle or may represent a metasomatic layer in the base of the lithosphere. There is no evidence for a contribution from the Afar mantle plume, as has been proposed elsewhere in northern Arabia. Melting during the Karacadağ and Ovabağ phases could have resulted from a combination of upwelling beneath weak or thinned lithosphere and restricted local extension of that weakened lithosphere as it collided with Eurasia. Tension associated with the collision focused magma of the Karacadağ phase into the elongate shield volcano of Mt. Karacadağ. The northern end of the fissure accommodated more extensive differentiation of magma, with isolated cases of crustal contamination, consistent with greater stress in the lithosphere closest to the collision. Most magma batches of the Karacadağ and Ovabağ phases differentiated by fractional crystallization at ~5 MPa, near the boundary between the upper and lower crust. Magma batches dominated by melt from garnet lherzolite show evidence for restricted amounts of differentiation at ~22·5 MPa, which is close to the base of the lithospheric mantle.

KEY WORDS: *Arabia; fissure volcano; intraplate; Karacadağ; Turkey*

INTRODUCTION

The Arabian Plate hosts several basaltic volcanic fields and so provides a valuable natural laboratory to explore intraplate magmatism (Camp & Roobol,. 1992; Ilani *et al.*, 2001; Shaw *et al.*, 2003; Krienitz *et al.*, 2006, 2007, 2009; Ma *et al.*, 2011). Intraplate magmatism occurred in clusters from 30 to 16 Ma and/or from 13 to 8 Ma in southern Turkey (e.g. Gaziantep, Kilis, Karacadağ; Gürsoy *et al.*, 2009; Lustrino *et al.*, 2010, 2012; Ekici *et al.*, 2012), in northern Syria (Krienitz *et al.*, 2006), associated with the Dead Sea Fault system in Syria (Ma *et al.*, 2011) and in the Harrat Ash Shaam (Shaw *et al.*, 2003; Krienitz *et al.*, 2007), with a significant increase in activity since Pliocene times (Ilani *et al.*, 2001). Most of this activity occurred close to and parallel to, although not always within, tectonic structures such as the Dead Sea Fault Zone, Euphrates Graben, Sirhan Graben, Karak Graben and Esdraelon Valley (Fig. 1a). Some of these structures, for example the Euphrates Graben, apparently experienced no tectonic activity during magmatism.

*Corresponding author. Telephone: +903462191010/1928. Fax: +902191171. E-mail: tanere7@gmail.com

The Karacadağ Volcanic Complex in SE Turkey (Fig. 1), sometimes referred to as Karacalıdağ, is one of a number of such volcanic fields distributed along the northern edge of the Arabian Plate where it has collided with Anatolia (Allen *et al.*, 2004). Until recently, magmatism from this complex was reported to be very young (Pearce *et al.*, 1990; Şen *et al.*, 2004). New geochronological data for the Siverek plateau lavas, which constitute the earliest activity of the complex, indicate that activity began no later than the Middle Miocene (Lustrino *et al.*, 2010, 2012; Ekici *et al.*, 2012). Petrogenetic models for the Karacadağ Volcanic Complex, and for other intraplate volcanic fields in northernmost Arabia, have tended to concentrate on the proximity of the Arabian–Anatolian collision in

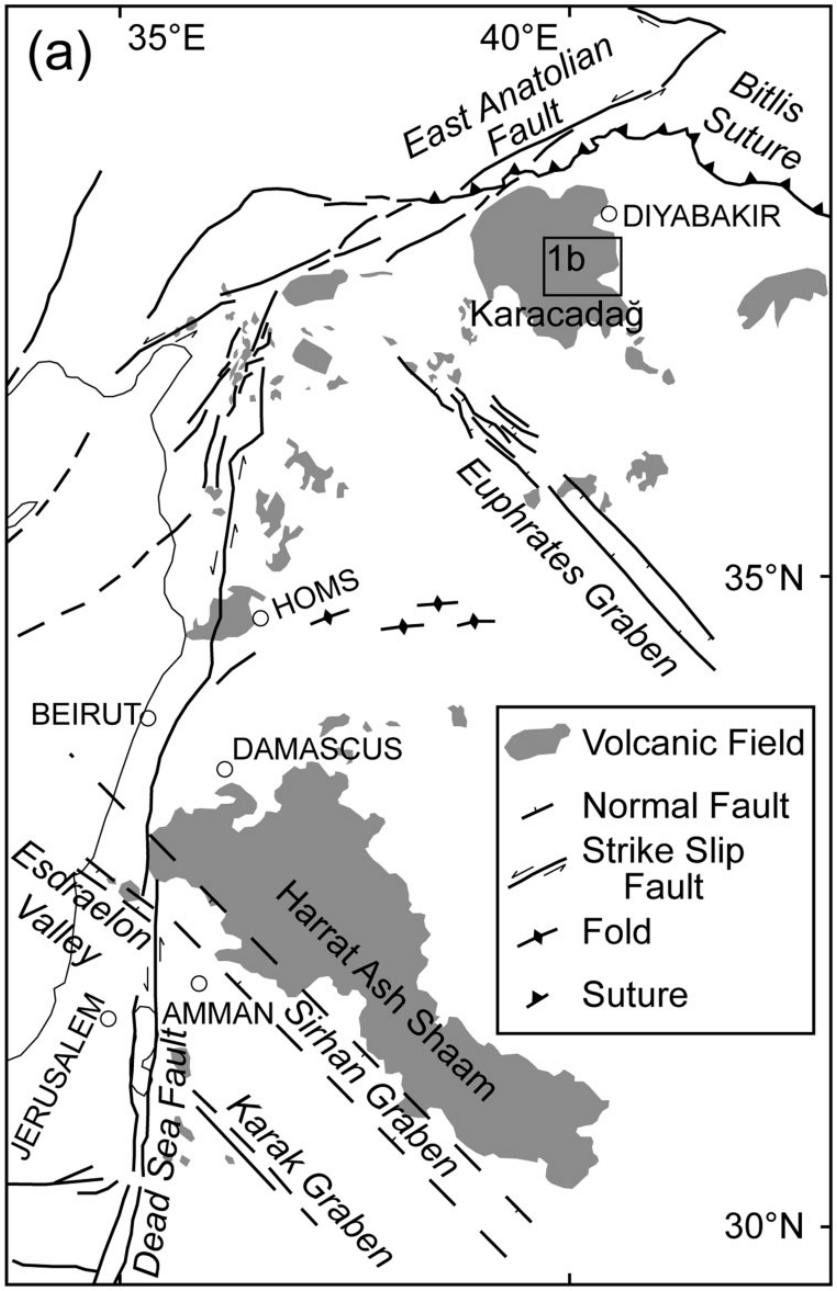

Fig. 1. (a) Location of the Karacadağ Volcanic Complex along with other Neogene to Quaternary volcanic fields at the northern margin of the Arabian Plate and the locations of major tectonic features in the region. The location of (b) is indicated. (b) Map of the Karacadağ Volcanic Complex showing the distribution of the Karacadağ and Ovabağ lavas and sites sampled during this work. Symbols are based on geochemical discrimination (see text for details).

(continued)

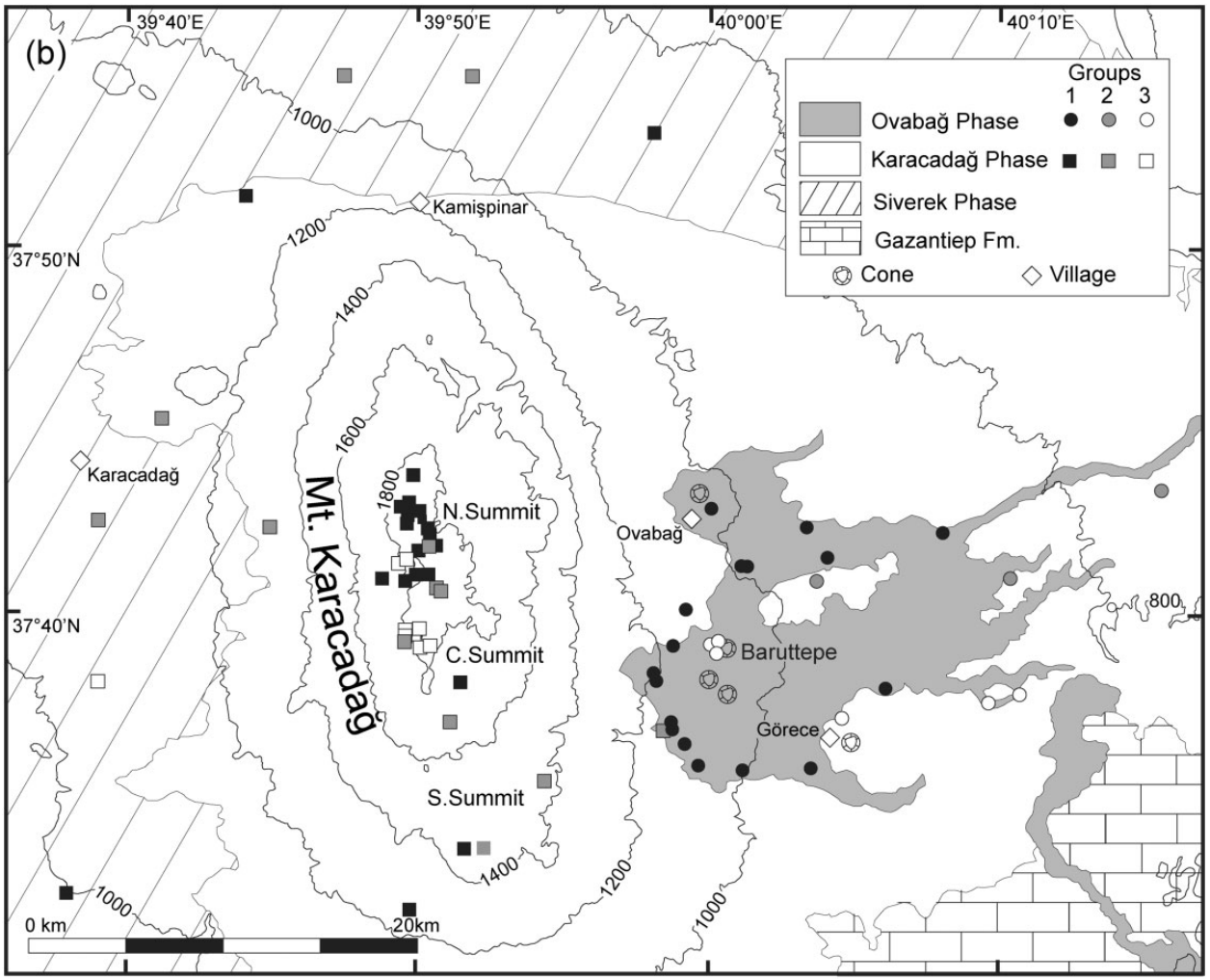

Fig. 1. Continued.

seeking a geodynamic context for the magmatism (e.g. Keskin, 2003; Krienitz *et al.*, 2006). The recognition of multiple phases of magmatism demonstrates that the Karacadağ Volcanic Complex is not the result of a single event or process. In a previous publication we discussed the petrogenesis of the Miocene Siverek plateau lavas (Ekici *et al.*, 2012). In this contribution we turn our attention to the younger magmatism. Lustrino *et al.* (2012) have shown this is geochemically distinct from the earlier Siverek phase. Our analysis reveals further levels of distinction within each of the two young phases of activity at the complex. We explore the petrogenesis of this magmatism in the context of tectonic activity associated with the developing collision and the structure of the Arabian Plate.

GEOLOGICAL SETTING

The Karacadağ Volcanic Complex, in SE Turkey, lies immediately south of the Arabian–Anatolian Collision Zone (Fig. 1). The collision is the result of northward motion of the Arabian Plate with respect to Eurasia and the Anatolian Plate (Allen *et al.*, 2004). During the Paleocene this caused Neo-Tethyan oceanic lithosphere to be subducted beneath Anatolia. Subduction continued until formation of the Bitlis Suture between Arabia and Anatolia (Fig. 1a). Continued convergence between Arabia and Eurasia led to westward extrusion of Anatolia along the Northern and Eastern Anatolian faults during the Late Miocene (Robertson, 2000; Şengör *et al.*, 2008).

The structure of the northernmost Arabian Plate is relatively poorly known, with most constraints coming from studies in Saudi Arabia, Jordan and Syria. Heat-flow measurements and xenolith petrology have been used to estimate that the lithosphere–asthenosphere transition occurs at ~80 km depth (McGuire & Bohannon, 1989; Nasir & Safarjalani, 2000; Shaw *et al.*, 2007). Seismic data suggest that below 35 km depth a mafic lower crust is

succeeded by a 5–8 km thick mantle transition zone (El-Isa *et al.*, 1987*a*, 1987*b*). Both petrological and seismic evidence indicate that the boundary between upper and lower crust lies close to 19 km beneath the surface (El-Isa *et al.*, 1987*b*; Nasir, 1992).

The Karacadağ Volcanic Complex has been active since the Middle Miocene when the Siverek phase plateau basalts were produced (Ercan *et al.*, 1990; Lustrino *et al.*, 2010; Ekici *et al.*, 2012) but is particularly well known for its Late Miocene to Quaternary products (Ercan *et al.*, 1990; Pearce *et al.*, 1990; Adıyaman & Chorowicz, 2002; Keskin, 2003; Şen *et al.*, 2004; Brigland *et al.*, 2007; Demir *et al.*, 2007; Lustrino *et al.*, 2010). This younger activity can be grouped into two further phases, termed Karacadağ and Ovabağ.

During the Late Miocene to Quaternary alkali basaltic and basanitic lavas were erupted from Mt. Karacadağ, a north–south-trending fissure volcano ~25 km in length. We refer to three summits on the volcanic axis as the northern, central and southern summits (Fig. 1b). Single lavas from Mt Karacadağ initially flowed east or west, extending up to 15 km to either side of the volcanic ridge. The lava fields also extend up to 25 km north and south of the fissure. Nine Ar–Ar age determinations yield ages ranging from 4·50 to 0·91 Ma (Ekici *et al.*, 2014), which agree with previous age determinations for Mt. Karacadağ (Pearce *et al.*, 1990; Lustrino *et al.*, 2010). Adıyaman & Chorowicz (2002) have suggested that the northern end of Mt. Karacadağ lies at the southern end of a WNW–ESE-trending fault extending from the East Anatolian Fault. The Karacadağ fissure indicates that the lithosphere was under tensional stress during this stage of the collision, although there is little evidence that this part of the northern margin of the Arabian Plate experienced significant east–west extension.

The products of the youngest phase of activity in the complex lie ~15 km to the east of Mt. Karacadağ, to the SE of the village of Ovabağ (Fig. 1b). These are predominantly alkali basalt flows erupted from monogenetic cones and cover an area of ~150 km^2. The youngest of these flows, erupted from the 100 m high Baruttepe cone, is exceptionally fresh, although there is little evidence of alteration of any of the Ovabağ flows. Most of these lavas were erupted from cones similar to Baruttepe and flowed east up to 20 km from the eastern flank of Mt. Karacadağ before being channelled into river valleys and flowing up to a further 5 km east or SE. The flows are vesicular and often retain flow structures such as pahoehoe surfaces and surface break-out structures. Vesicles are generally empty and only rarely contain secondary calcite. Similar monogenetic cones occur further to the east and south of the Karacadağ Volcanic Complex, towards the border with Syria. Ekici *et al.* (2014) obtained Ar–Ar ages of 0·29 ± 0·13 and 0·53 ± 1·14 Ma for an Ovabağ lava, which is consistent with geomorphological evidence for very recent activity.

ANALYTICAL METHODS

Seventy-six fresh samples, 48 from Mt. Karacadağ and 28 from Ovabağ, were analysed for their major and trace element concentrations at ACME laboratories, Canada (Table 1 and Supplementary Data Table 3; all supplementary data are available for downloading at http://www.petrology.oxfordjournals.org). Any calcite-bearing vesicles were avoided when preparing material for analysis. Major element analyses were conducted by X-ray fluorescence upon fused discs prepared by using six parts of lithium tetraborate and one part of rock powder. The mixture was fused in crucibles of 95% Pt and 5% Au at 1050°C for 60 min to form a homogeneous melt that was cast into a thick glass disc. Trace element concentrations were analysed by inductively coupled plasma mass spectrometry (ICP-MS) using a fusion method. Precision was monitored using an internal standard (SO-18) and accuracy was calibrated using standards W-2, GSP-2, BCR-2, SY4 and SY-3 (Supplementary Data Tables 1 and 2). The uncertainty on these measurements is better than ±3% for major element oxides and ±10% for trace elements.

Isotope ratios of Pb, Sr, and Nd were measured on splits separated from the same 0·2 g aliquots at the University of Geneva using a seven-collector Finnigan MAT 262 thermal ionization mass spectrometer during December 2008. Samples were processed using procedures described by Chiaradia *et al.* (2011). The 90° magnetic sector mass analyser has an extended geometry with stigmatic focusing. $^{87}Sr/^{86}Sr$ and $^{143}Nd/^{144}Nd$ ratios were measured in semi-dynamic mode, using double Re filaments. Conventional Pb isotope ratio measurements were obtained in dynamic mode with a single Re filament. $^{88}Sr/^{86}Sr = 8{\cdot}375209$ was used to correct the mass fractionation of $^{87}Sr/^{86}Sr$, which was compared with the NIST-SRM987 $^{87}Sr/^{86}Sr$ value of 0·710240 [$^{87}Sr/^{86}Sr_{measured} = 0{\cdot}710240 \pm 0{\cdot}000012$ (2σ), $n = 31$]. $^{143}Nd/^{144}Nd$ was mass fractionation corrected relative to a $^{146}Nd/^{144}Nd$ value of 0·721903 and normalized to the Nd La Jolla standard value of 0·511835 [$^{143}Nd/^{144}Nd_{measured} = 0{\cdot}511845 \pm 0{\cdot}000004$ (2σ), $n = 26$]. Lead isotope data were corrected for instrumental mass fractionation and machine bias by applying a discrimination factor determined by multiple analyses of NBS SRM981, using the reference value of Todt *et al.* (1984). The discrimination factor averaged 0·00082 ± 0·00005 (2 SE, $n = 132$) per mass unit. External reproducibility (2σ) of the standard ratios is 0·05% for $^{206}Pb/^{204}Pb$, 0·08% for $^{207}Pb/^{204}Pb$ and 0·10% for $^{208}Pb/^{204}Pb$. These standard analyses were performed during a 6 month period in which the Karacadağ lavas were analysed. Pb, Sr and Nd blanks were all below their respective detection limits.

Table 1: Major and trace element compositions of Karacadağ and Ovabağ lavas

Sample:	DK-1 (K1)	DK-8 (K1)	DK-10 (K1)	DK-11 (K2)	DK-16 (K1a)	DK-19 (K1)	DK-22 (K3)	DK-23 (K2)
Latitude (N):	37°42′35·64″	37°42′5·22″	37°41′46·80″	37°41′46·08″	37°40′51·24″	37°41′18·74″	37°39′5·76″	37°39′13·44″
Longitude (E):	39°49′43·20″	39°50′27·12″	39°50′34·80″	39°50′26·16″	39°49′39·24″	39°49′57·09″	39°50′12·30″	39°49′39·48″
SiO_2	46·15	48·34	49·04	45·86	47·05	51·11	41·80	45·44
TiO_2	3·04	2·67	2·24	2·79	3·60	1·79	3·43	2·61
Al_2O_3	15·38	17·22	17·70	14·33	16·23	17·82	13·01	14·27
Fe_2O_3	13·49	12·11	11·12	12·93	12·33	10·88	14·93	14·68
MgO	6·55	4·08	2·92	8·81	5·10	2·25	9·92	9·65
MnO	0·17	0·17	0·18	0·16	0·15	0·19	0·18	0·17
CaO	10·10	6·75	6·57	8·79	8·36	5·52	8·60	8·91
Na_2O	3·46	4·96	5·33	3·33	3·90	5·95	4·43	3·08
K_2O	1·06	2·13	2·49	1·30	2·07	2·70	1·87	0·67
P_2O_5	0·42	0·83	0·87	0·47	0·52	0·99	0·96	0·32
Cr_2O_3	0·019	0·007	0·002	0·046	0·012	0·002	0·027	0·038
LOI	−0·2	0·4	1·2	0·8	0·3	0·5	0·3	−0·2
Total	99·65	99·67	99·63	99·63	99·65	99·69	99·49	99·66
Ni	72	28	20	132	51	20	206	223
Sc	24	11	7	21	17	9	17	21
V	293	139	152	260	295	44	247	246
Co	79·7	46·1	42·1	74·0	60·3	47·9	76·7	79·5
Cu	64·5	31·0	22·6	41·0	43·5	15·3	43·5	81·3
Zn	82	83	88	76	87	99	74	93
Ga	23·2	24·9	23·8	22·4	25·7	26·6	26·5	20·5
Rb	11·1	16·8	22·8	10·4	27·8	24·7	17·5	6·3
Sr	678	1048	1267	707	793	991	1192	530
Y	21·1	23·8	26·2	20·6	23·8	26·7	22·1	16·9
Zr	173	323	421	193	235	375	315	109
Nb	28·4	48·5	60·9	33·6	42·4	62·2	63·6	18·3
Cs	0·3	0·2	0·2	0·2	0·6	0·3	0·2	0·1
Ba	179	237	250	186	306	343	248	124
La	21·1	39·7	50·1	24·1	30·0	51·9	51·0	13·2
Ce	47·7	85·0	102·8	52·1	64·5	107·3	104·4	30·2
Pr	6·11	10·33	12·19	6·42	8·08	12·84	12·75	4·00
Nd	26·1	41·0	47·6	26·2	34·0	49·8	51·8	17·7
Sm	5·76	7·86	8·82	5·71	7·15	8·93	9·76	4·37
Eu	2·14	2·85	2·92	2·06	2·38	2·97	3·32	1·62
Gd	5·95	7·31	7·69	5·63	6·78	7·77	8·58	4·46
Tb	0·92	1·04	1·10	0·86	1·02	1·12	1·17	0·70
Dy	4·49	5·15	5·31	4·25	4·95	5·29	5·03	3·44
Ho	0·84	0·89	0·99	0·76	0·86	0·98	0·82	0·64
Er	2·00	2·25	2·36	1·90	2·19	2·30	1·70	1·48
Tm	0·31	0·34	0·36	0·26	0·31	0·35	0·24	0·22
Yb	1·60	1·79	2·05	1·53	1·74	2·05	1·29	1·21
Lu	0·26	0·27	0·31	0·22	0·26	0·30	0·17	0·17
Hf	4·4	7·4	9·3	4·6	5·7	8·0	7·1	2·7
Ta	1·6	2·8	3·6	2·0	2·4	3·6	3·4	1·0
Pb	2·0	0·7	3·1	0·9	2·9	1·9	1·7	0·8
Th	2·1	3·4	5·1	2·2	4·1	4·5	4·7	1·1
U	0·7	1·3	1·4	0·7	1·2	1·7	1·8	0·4

(continued)

Table 1: Continued

Sample:	DK-25 (K3)	DK-26 (K3)	DK-27 (K3)	DK-29 (K2)	DK-30 (K2)	DK-52 (K2)	DK-58 (K1a)	DK-93 (K1)
Latitude (N):	37°39′30·42″	37°39′28·98″	37°39′26·10″	37°40′35·82″	37°40′40·32″	37°42′31·26″	37°53′10·32″	37°33′45·60″
Longitude (E):	39°49′40·56″	39°50′9·78″	39°50′6·66″	39°50′52·02″	39°50′42·84″	39°38′59·04″	39°57′57·24″	39°51′39·24″
SiO_2	42·60	42·60	43·02	47·07	46·26	44·90	47·03	46·24
TiO_2	3·13	3·35	3·28	2·58	2·84	2·48	2·80	2·99
Al_2O_3	13·71	13·30	13·39	14·83	14·65	13·64	14·94	15·30
Fe_2O_3	15·27	14·56	15·57	12·86	13·54	14·67	12·60	13·93
MgO	5·43	10·25	6·48	7·60	8·21	10·09	6·28	5·71
MnO	0·20	0·17	0·19	0·18	0·18	0·17	0·15	0·17
CaO	7·51	8·85	7·10	7·70	8·20	9·32	9·71	9·92
Na_2O	5·07	3·73	5·69	4·09	3·86	2·97	3·44	3·70
K_2O	2·86	1·60	2·92	1·76	1·65	0·80	1·37	1·18
P_2O_5	1·17	0·76	1·14	0·77	0·76	0·35	0·39	0·57
Cr_2O_3	0·010	0·037	0·010	0·036	0·041	0·040	0·030	0·018
LOI	2·5	0·3	0·7	0·1	0·1	0·2	1·0	−0·1
Total	99·45	99·54	99·49	99·60	100·2	99·65	99·72	99·67
Ni	76	225	99	129	151	223	106	78
Sc	8	19	7	16	18	202	260	21
V	155	265	163	189	217	258	258	281
Co	102·4	87·7	60·2	62·2	67·8	80·1	58·7	62·1
Cu	29·4	62·1	25·0	47·9	56·5	67·8	50·6	56·7
Zn	127	103	100	85	92	92	72	81
Ga	32·0	24·8	31·0	24·1	23·2	20·3	21·0	24·0
Rb	27·5	11·7	28·1	14·7	14·0	8·0	20·1	12·3
Sr	1628	1020	1511	816	810	579	580	758
Y	25·2	20·7	22·8	23·2	22·0	17·2	20·4	23·1
Zr	501	248	482	282	260	130	177	183
Nb	102·5	45·8	92·3	42·6	41·1	20·6	22·9	31·2
Cs	0·4	0·2	0·4	0·1	0·2	0·1	0·5	0·2
Ba	409	192	358	266	228	202	260	185
La	74·8	37·4	67·8	37·2	34·2	17·3	21·5	24·7
Ce	155·8	81·0	141·4	75·0	72·3	38·6	47·0	51·8
Pr	18·88	10·00	17·39	9·34	8·80	4·96	6·00	6·76
Nd	74·0	40·7	68·9	36·2	36·0	20·9	25·5	30·1
Sm	13·50	8·53	12·90	7·11	7·09	4·74	5·43	6·16
Eu	4·38	2·78	4·13	2·43	2·33	1·71	1·85	2·18
Gd	11·26	7·53	10·76	6·52	6·30	4·76	5·43	5·72
Tb	1·44	1·04	1·35	0·93	0·94	0·75	0·81	0·90
Dy	5·80	4·78	5·76	4·39	4·18	3·61	4·23	4·90
Ho	0·95	0·79	0·86	0·82	0·83	0·68	0·73	0·83
Er	1·88	1·76	1·64	2·09	1·92	1·69	1·82	2·05
Tm	0·24	0·25	0·20	0·29	0·27	0·24	0·28	0·29
Yb	1·28	1·29	1·07	1·69	1·64	1·29	1·59	1·60
Lu	0·17	0·18	0·14	0·24	0·25	0·23	0·27	0·23
Hf	11·1	5·7	10·9	6·6	5·9	3·7	4·6	4·8
Ta	5·5	2·6	5·0	2·4	2·3	1·2	1·4	1·7
Pb	4·4	2·3	1·3	2·0	1·5	1·5	2·7	1·5
Th	6·6	2·9	5·7	3·4	2·7	1·9	2·5	2·6
U	2·3	1·1	2·3	1·2	1·1	0·6	0·8	0·7

(continued)

Table 1: Continued

Sample:	DK-99 (K3)	DK-102 (K2)	DO-59 (O1)	DO-62 (O2)	DO-63 (O1)	DO-64 (O3)	DO-66 (O3)	DO-67 (O3)
Latitude (N):	37°38′13·32″	37°42′24·60″	37°41′24·84″	37°41′5·04″	37°41′42·24″	37°39′11·34″	37°39′7·20″	37°39′7·62″
Longitude (E):	39°39′9·06″	39°44′58·02″	40°1′10·20″	40°3′46·80″	40°4′7·08″	40°0′4·38″	40°0′29·10″	40°0′29·34″
SiO_2	41·96	44·91	47·29	46·50	47·41	44·18	44·48	44·95
TiO_2	3·42	2·65	2·31	2·67	2·47	3·32	2·88	2·73
Al_2O_3	13·08	13·52	13·22	14·53	13·61	13·43	13·14	13·22
Fe_2O_3	15·29	14·55	12·78	13·66	13·17	14·91	14·76	14·29
MgO	8·94	9·84	10·44	8·22	9·88	9·95	9·52	9·66
MnO	0·18	0·19	0·16	0·17	0·16	0·18	0·17	0·17
CaO	9·03	9·00	8·55	8·98	8·35	9·10	8·57	8·61
Na_2O	4·17	3·19	3·06	3·45	3·06	4·03	3·94	3·77
K_2O	0·84	1·02	1·21	1·51	1·27	1·80	1·74	1·62
P_2O_5	0·98	0·46	0·43	0·47	0·46	0·70	0·71	0·61
Cr_2O_3	0·030	0·041	0·049	0·038	0·044	0·032	0·032	0·035
LOI	1·6	0·2	0·1	-0·2	−0·3	0·0	−0·4	−0·1
Total	99·53	99·61	99·64	99·65	99·63	101·65	99·57	99·60
Ni	191	227	242	110	231	181	176	191
Sc	16	20	21	21	21	19	19	20
V	279	273	229	260	237	267	240	235
Co	69·3	79·9	70·4	64·6	72·9	82·5	74·5	74·3
Cu	44·8	59·7	41·9	46·3	54·5	52·1	45·1	49·1
Zn	99	77	65	91	85	94	99	65
Ga	25·9	21·1	20·6	22·4	22·1	24·9	24·5	22·8
Rb	5·4	10·8	18·1	14·0	17·7	15·7	19·1	18·7
Sr	1302	737	568	678	610	949	878	814
Y	21·5	19·6	20·0	24·4	21·8	24·7	24·7	24·4
Zr	324	171	162	187	178	267	240	235
Nb	52·5	26·4	26·3	30·9	29·4	57·2	52·8	47·0
Cs	0·2	0·2	0·8	0·3	0·8	0·2	0·4	0·4
Ba	205	191	202	216	228	258	272	254
La	44·7	21·6	23·1	27·3	25·9	41·8	43·2	37·0
Ce	91·9	45·6	48·3	56·5	53·0	86·0	85·1	72·9
Pr	12·10	6·05	6·14	7·32	6·84	10·87	10·67	9·39
Nd	47·7	26·1	25·2	31·6	28·2	44·7	42·7	37·4
Sm	9·55	5·44	5·33	6·13	5·78	8·56	8·01	7·08
Eu	3·18	1·95	1·90	2·27	1·98	2·86	2·73	2·41
Gd	7·99	5·00	5·35	6·31	5·83	8·13	7·81	7·09
Tb	1·11	0·80	0·82	0·94	0·88	1·14	1·11	1·03
Dy	5·28	3·95	4·18	4·91	4·60	5·42	5·41	5·07
Ho	0·77	0·68	0·76	0·90	0·83	0·93	0·94	0·90
Er	1·81	1·68	1·83	2·18	1·98	2·10	2·15	2·15
Tm	0·22	0·23	0·27	0·33	0·31	0·31	0·32	0·32
Yb	1·14	1·26	1·55	1·87	1·66	1·70	1·81	1·75
Lu	0·17	0·19	0·25	0·30	0·28	0·27	0·29	0·28
Hf	7·9	4·1	4·1	4·8	4·5	6·7	6·2	5·7
Ta	3·1	1·6	1·6	1·9	1·8	3·4	3·1	2·7
Pb	2·4	1·5	2·1	2·7	2·8	2·6	2·1	2·1
Th	4·7	3·9	3·0	3·0	2·9	3·6	4·5	3·7
U	1·4	0·7					1·4	1·2

(continued)

Table 1: Continued

Sample:	DO-68 (O1)	DO-71 (O1)	DO-78 (O3)	DO-107 (O1)	DO-110 (O2)	DO-113 (O2)	DO-114 (O3)
Latitude (N):	37°42′28·62″	37°38′13·32″	37°37′47·04″	37°37′1·62″	37°43′27·18″	37°41′6·34″	37°40′17·88″
Longitude (E):	40° 8′10·98″	39°58′14·22″	40°10′58·26″	39°58′37·74″	40°15′38·34″	40°10′23·70″	40°13′52·50″
SiO_2	46·28	47·26	45·88	46·73	47·60	48·37	45·07
TiO_2	2·76	2·52	2·43	2·50	2·04	2·26	2·76
Al_2O_3	13·97	13·23	12·79	13·62	14·35	13·87	13·12
Fe_2O_3	13·55	13·36	13·63	13·22	13·74	13·45	13·65
MgO	9·44	10·06	11·25	10·35	9·12	8·81	10·42
MnO	0·16	0·16	0·17	0·17	0·17	0·17	0·18
CaO	8·25	8·34	8·73	8·56	8·52	8·33	9·15
Na_2O	3·37	3·27	3·16	3·12	2·88	3·26	3·15
K_2O	1·33	1·20	1·20	1·23	0·72	1·12	1·50
P_2O_5	0·53	0·43	0·46	0·44	0·28	0·36	0·62
Cr_2O_3	0·046	0·045	0·043	0·046	0·046	0·044	0·038
LOI	−0·1	−0·3	−0·2	−0·4	0·2	−·4	−0·1
Total	99·62	99·62	99·58	99·64	99·67	99·67	99·59
Ni	194	235	251	246	185	165	221
Sc	19	20	21	21	23	23	22
V	242	233	221	221	229	227	260
Co	69·8	73·1	71·3	78·4	76·8	66·7	88·9
Cu	53·9	58·9	57·7	50·2	37·3	40·2	44·3
Zn	88	92	91	80	77	79	75
Ga	21·2	21·4	20·7	21·0	21·1	20·9	22·3
Rb	13·8	16·6	15·3	15·3	5·6	17·3	19·1
Sr	705	625	637	583	401	487	859
Y	20·5	22·1	20·8	20·0	20·7	20·9	23·2
Zr	242	172	168	173	137	156	211
Nb	27·5	29·1	34·7	29·4	16·0	21·7	48·1
Cs	0·2	0·5	0·2	0·5	0·1	0·2	0·2
Ba	209	209	377	212	225	205	294
La	28·6	26·3	22·8	22·4	15·9	20·3	34·6
Ce	58·4	52·0	51·0	47·1	34·8	43·6	70·0
Pr	7·4	6·90	6·50	6·44	4·74	5·87	9·00
Nd	31·8	28·6	27·2	27·7	21·8	26·0	37·0
Sm	5·92	5·75	5·50	5·96	4·85	5·50	7·44
Eu	2·15	2·02	1·94	1·90	1·55	1·68	2·23
Gd	5·88	5·73	5·51	5·56	4·66	5·04	6·56
Tb	0·85	0·88	0·83	0·84	0·77	0·83	0·95
Dy	4·20	4·50	4·30	4·21	4·04	4·29	4·69
Ho	0·75	0·79	0·77	0·78	0·78	0·84	0·84
Er	1·83	1·93	1·89	1·99	2·19	2·13	2·29
Tm	0·28	0·29	0·28	0·24	0·29	0·29	0·30
Yb	1·48	1·64	1·52	1·49	1·63	1·72	1·54
Lu	0·24	0·26	0·24	0·21	0·26	0·26	0·24
Hf	5·1	4·6	4·3	4·7	4·0	4·7	5·3
Ta	1·7	1·8	2·0	1·9	1·1	1·4	2·9
Pb	1·0	2·4	2·3	2·1	1·9	1·5	2·2
Th	2·3	2·9	3·3	2·7	3·0	4·2	4·4
U	0·8	0·9	0·8	0·7	0·3	0·6	1·2

PETROGRAPHY OF THE LAVAS

All the lavas from Mt. Karacadağ are alkaline, including alkali basalts, trachybasalts, basanites and tephrites, with rare phonotephrites. Most lavas are very fresh, the vast majority having low loss on ignition (LOI) values of less than 1% (Table 1 and Supplementary Data Table 3). The lavas are fine grained and porphyritic, containing olivine and plagioclase phenocrysts, up to 25 modal %, set in a matrix of the same minerals, plus clinopyroxene, which is occasionally titanium-rich, and Fe–Ti oxides. Phenocrysts are generally 0·2–1 mm in size with groundmass crystals less than 0·1 mm. Plagioclase phenocrysts show some signs of disequilibrium, with sieve textures observed in a number of samples. Such disequilibrium might arise from magma mixing or crustal contamination (Dungan & Rhodes, 1978) but could also result from decompression or heating (Nelson & Montana, 1992; Thy *et al.*, 2013). Therefore, the sieve textures, in themselves, do not provide evidence for open-system behaviour.

Lavas from Ovabağ are exceptionally fresh as shown by their very low, and frequently positive, LOI, which is due to iron oxidation during ignition. These lavas include basalts, alkali basalts, trachybasalts and rare tephrites. Like the Karacadağ phase lavas these are fine-grained but differ in the predominance of olivine phenocrysts. Again, there is a range of phenocryst contents, up to 25 modal %. Titanaugite is more common than at Karacadağ, sometimes as micro-phenocrysts, but usually as part of the groundmass.

GEOCHEMISTRY OF THE LAVAS

Lavas from both volcanic phases can be split into three groups based on their geochemistry. In the discussion below these are referred to as groups K1, K2 and K3 for the Karacadağ phase and O1, O2 and O3 for the Ovabağ phase. Similarities between the Karacadağ and Ovabağ groups are noted where appropriate.

Karacadağ phase

Lavas from both the Karacadağ and Ovabağ phases show similar ranges in major and trace element compositions to those reported in earlier studies (Figs 2 and 3). Karacadağ phase lavas display a much wider range in composition than those from Ovabağ. Group K1 lavas have lower MgO (2·2–6·7 wt %) and higher Al_2O_3 (>15 wt %) than the other two Karacadağ groups (Fig. 2). In groups K2 and K3 MgO is generally greater than 8 wt %, but K3 is offset to lower SiO_2 and Al_2O_3 and to higher TiO_2, Fe_2O_3, Na_2O, K_2O and P_2O_5 for a given MgO content. Most major element oxides correlate well with MgO, particularly in group K1, although Fe_2O_3 and TiO_2 display more scatter than other oxides owing to an inflection at around 5 wt % MgO. The major element groupings of the Karacadağ phase are also readily apparent in their trace element concentrations. Nickel contents of K2 and K3 lavas are similar to one another and significantly greater than those of K1 (Table 1 and Supplementary Data Table 3). Within each group of the Karacadağ phase concentrations of incompatible elements increase with decreasing MgO (Fig. 3).

In mantle-normalized trace element diagrams all Karacadağ phase lavas show patterns that are enriched in the most incompatible elements, peaking at Nb, and depleted in the heavy rare earth elements (HREE) and Y (Fig. 4). A striking negative Pb anomaly is apparent in the patterns of all groups. Patterns for K1 and K2 lavas are very similar but with greater concentrations in the former, consistent with their lower MgO contents. Group K3 lavas have more elevated concentrations of incompatible elements than those from group K2 (Fig. 2) but with similar shaped patterns (Fig. 4b and c), except for the presence of negative K anomalies in most K3 samples. The magnitude of this anomaly is not linked to MgO content, but is more pronounced in silica-poor rocks (Fig. 5a and b).

Group K3 lavas have the lowest values of $^{87}Sr/^{86}Sr$ and Δ7/4Pb and Δ8/4Pb, and the highest values of $^{143}Nd/^{144}Nd$ (Table 2 and Fig. 6) of any lava from the Karacadağ Volcanic Complex. Isotopic compositions for the other two Karacadağ groups largely overlap one another; a K1 sample (DK-58) has the most radiogenic Sr and least radiogenic Nd isotopic composition in this study. However, these values are not as extreme as those of the Miocene Siverek plateau lavas (Fig. 6). With the exception of DK-58, the ranges of isotopic compositions are similar to those previously observed for intra-plate magmatism elsewhere in the northern Arabian Plate (Shaw *et al.*, 2003; Krienitz *et al.*, 2009; Ma *et al.*, 2011).

Ovabağ phase

All Ovabağ lavas contain more than 8 wt % MgO. Group O1 lavas have higher SiO_2 and Al_2O_3, and lower CaO, Fe_2O_3, TiO_2, K_2O and Na_2O than O3 lavas at similar MgO. The restricted ranges in composition make it difficult to resolve systematic variations of other major elements with MgO within each group. Group O2 lavas are relatively scarce in our dataset and have the highest SiO_2 and lowest K_2O, TiO_2 and Na_2O for any MgO content in the Ovabağ phase (Fig. 2). Groups O1 and O3 display parallel, negative correlations between MgO and Ni (not shown), whereas O3 lavas are consistently enriched in incompatible elements compared with O1 at a given MgO content (Fig. 3). Group O2 lavas have the lowest incompatible element contents of the Ovabağ groups.

Comparing the Ovabağ and Karacadağ phases with one another, concentrations of major and incompatible trace elements in Group O1 lavas most closely resemble Group K2 but with slightly higher SiO_2 and K_2O (and most incompatible trace elements), and lower Fe_2O_3 and TiO_2

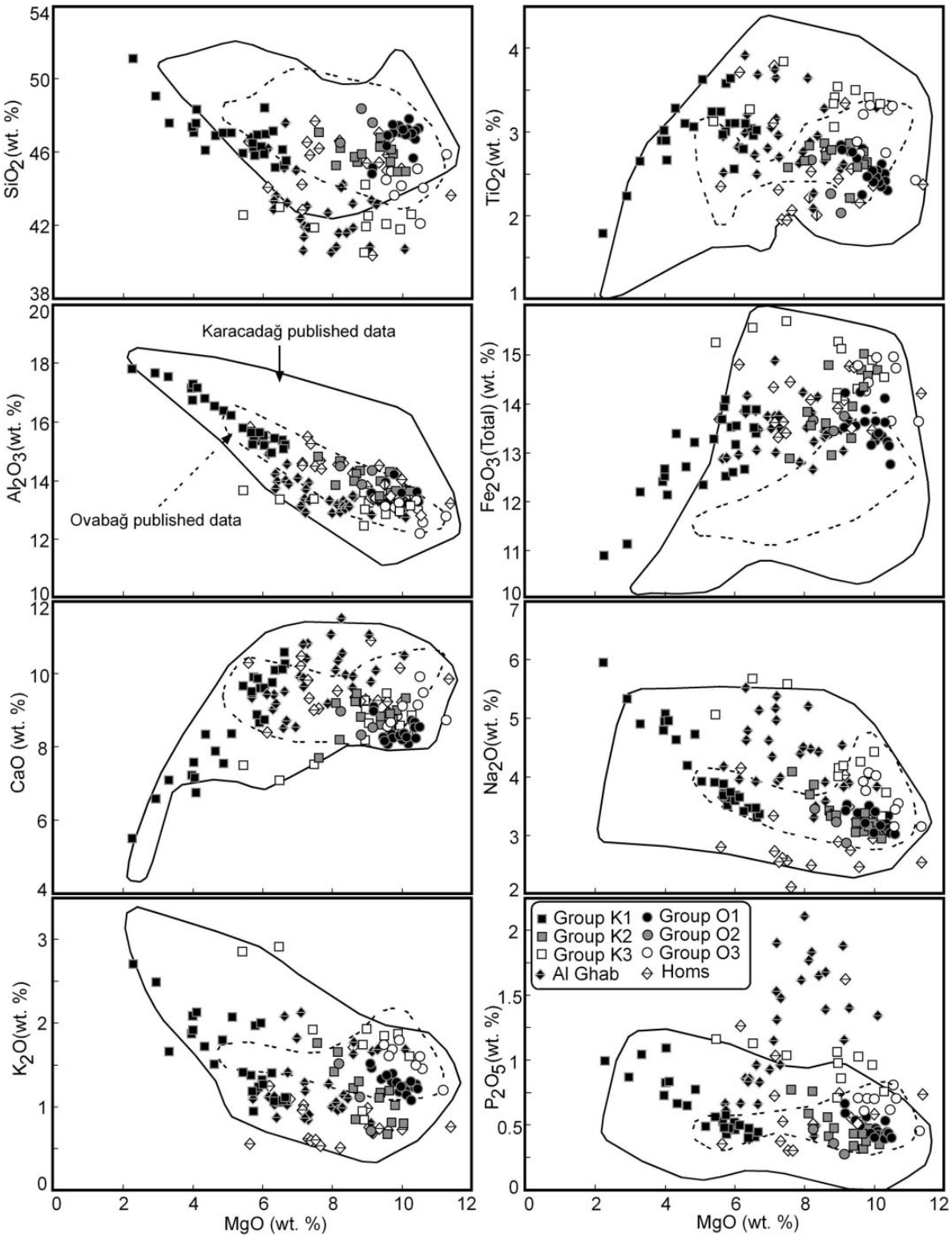

Fig. 2. Variation of selected major elements vs MgO for Karacadağ and Ovabağ phase lavas from the Karacadağ Volcanic Complex. Fields of published data for both phases are from Lustrino *et al.* (2012) and references therein. Data for Al Ghab and Homs volcanic fields within the northern Dead Sea Fault zone are from Ma *et al.* (2011).

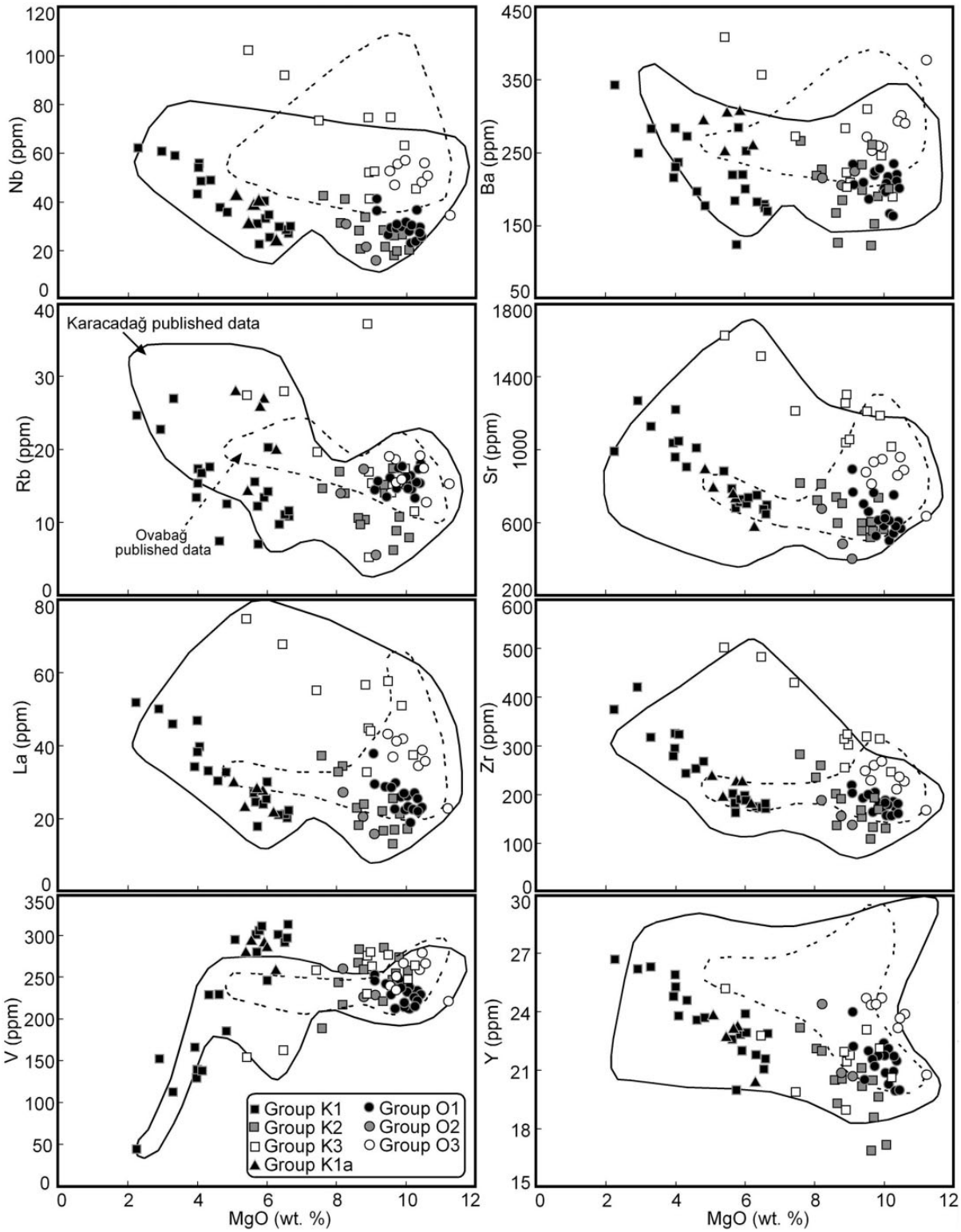

Fig. 3. Variation of selected trace elements vs MgO for the Karacadağ and Ovabağ phase lavas from the Karacadağ Volcanic Complex. Fields of published data for both phases are from Lustrino *et al.* (2012) and references therein. Data for Al Ghab and Homs volcanic fields within the northern Dead Sea Fault zone are from Ma *et al.* (2011).

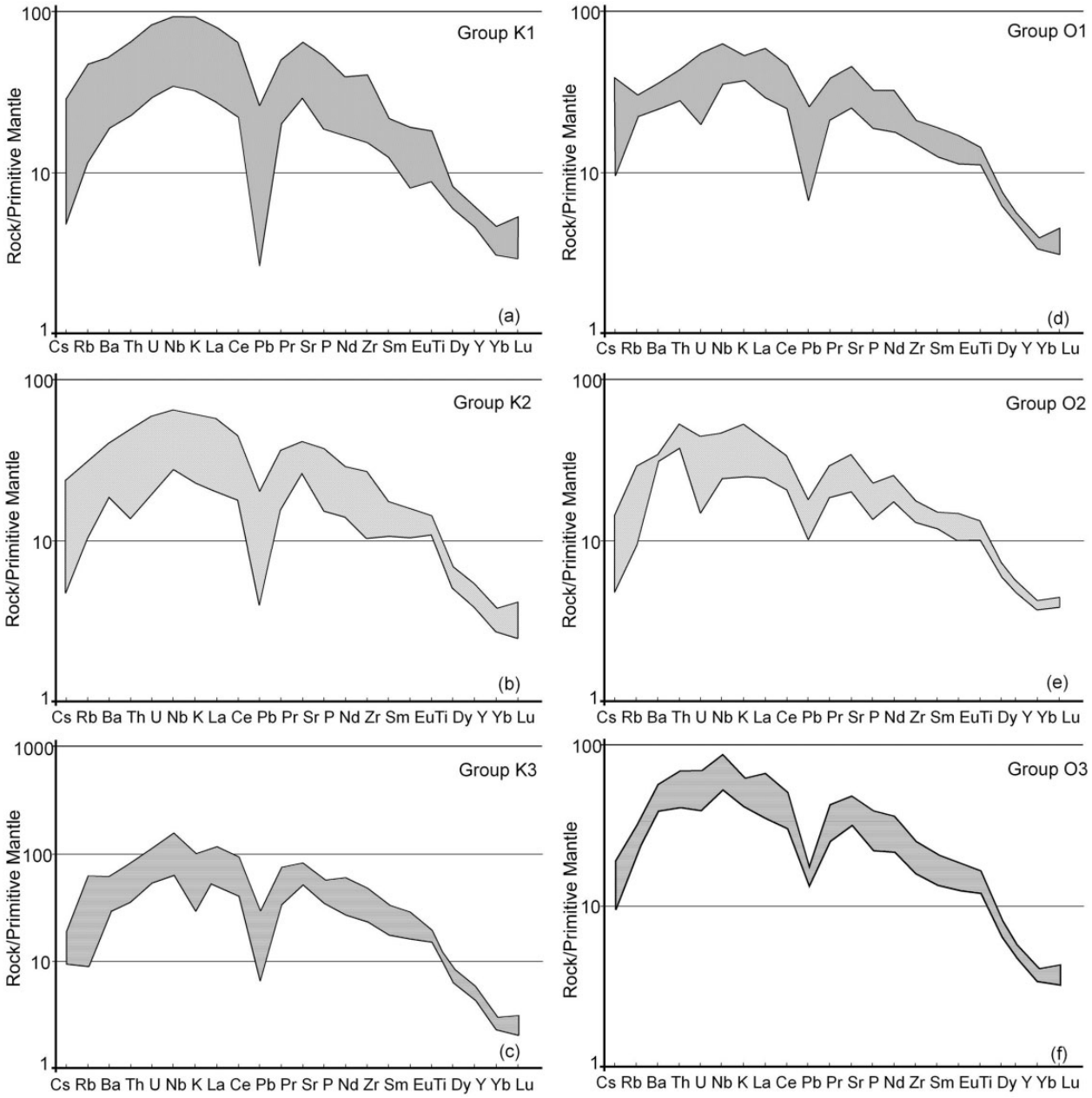

Fig. 4. Ranges of incompatible trace element concentrations in Karacadağ Volcanic Complex lavas normalized to primitive mantle (McDonough & Sun, 1995). Karacadağ phase: (a) group K1; (b) group K2; (c) group K3. [Note the more expanded scale in (c).] Ovabağ phase: (d) group O1; (e) group O2; (f) group O3.

(Figs 2 and 3). Several O1 lavas also show minor, positive K anomalies (Fig. 5b). The shapes of the O2 group multi-element patterns are similar to those of O1 but, as noted above, they have lower concentrations of all incompatible elements (Fig. 4). The greatest distinction of group O3 from the other Ovabağ lavas is their negative K anomalies, which are not as pronounced as those seen in group K3 but are, again, associated with lower silica contents (Fig. 5b). Lavas from groups K3 and O3 are very similar with respect to many major and trace elements (Figs 2 and 3) and trace element ratios (Figs 4 and 5).

Lavas from the Ovabağ phase of magmatism display more restricted ranges of radiogenic isotope compositions than the Karacadağ phase (Table 2). The lowest $^{87}Sr/^{86}Sr$ and highest $^{143}Nd/^{144}Nd$ occur in group O3, with values approaching those of group K3 (Fig. 6). A lava from group O1 (DO-68) has Sr, Nd and Pb isotopic compositions that lie within the range of the K1 and K2 lavas.

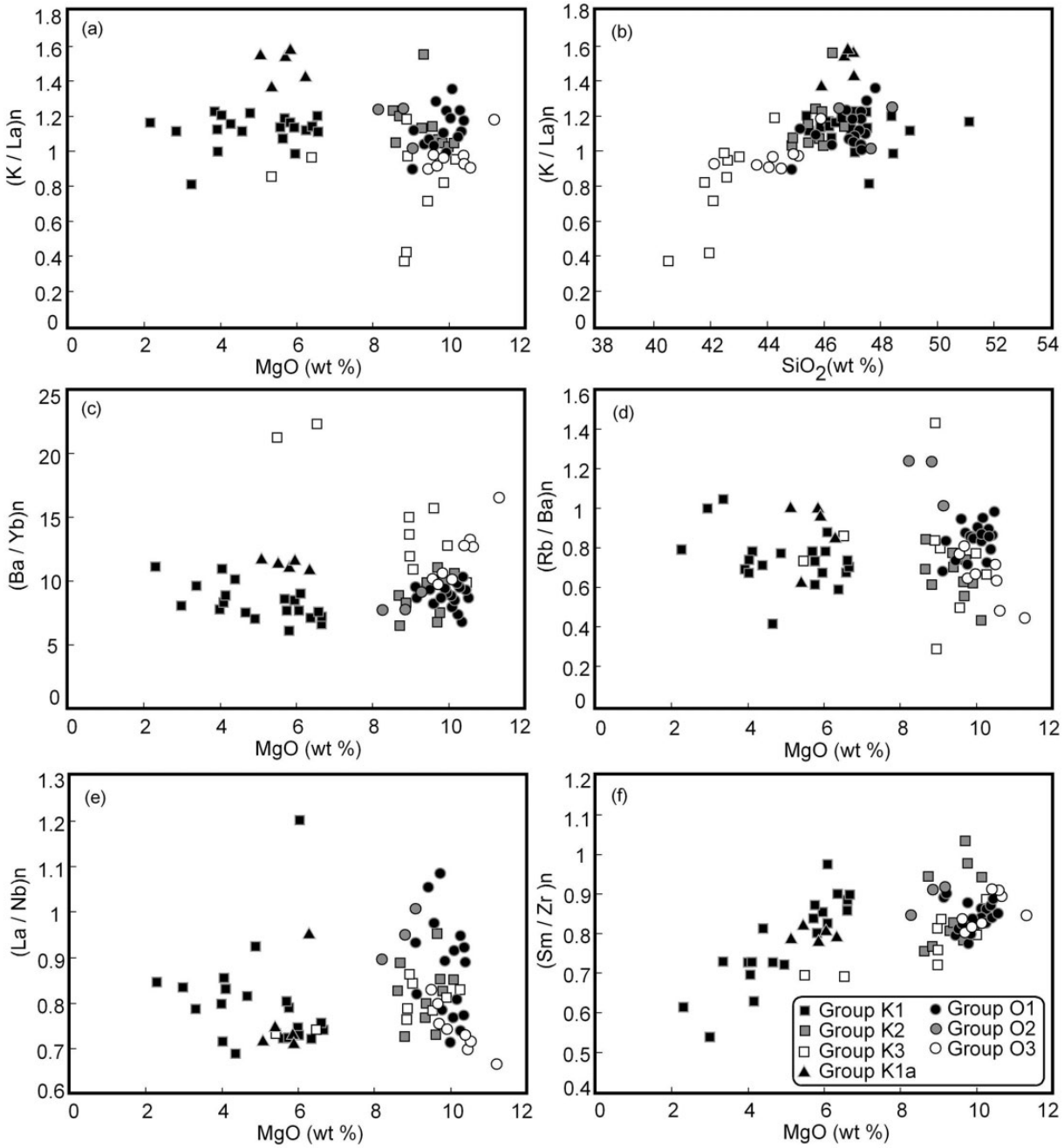

Fig. 5. Variation of selected incompatible trace element ratios vs MgO or SiO_2 normalized to primitive mantle (McDonough & Sun, 1995) for Karacadağ and Ovabağ phase lavas from the Karacadağ Volcanic Complex.

The remaining Ovabağ lavas have isotopic compositions that lie within the range previously observed for other northern Arabian intraplate volcanic fields (Fig. 6).

DISCUSSION

The existence of multiple magmatic phases within the Karacadağ Volcanic Complex has only been recently identified (Lustrino *et al.*, 2010; Ekici *et al.*, 2012). Previously, the complex was regarded as having a short magmatic history (e.g. Pearce *et al.* 1990; Keskin, 2003). Lustrino *et al.* (2012) recognized differences between the major and trace element geochemistry of the Karacadağ and Ovabağ phase lavas and attributed this to a long-term secular change in mantle source composition that included the preceding Siverek plateau lavas. The range

Table 2: Karacadağ and Ovabağ Sr–Nd–Pb isotopic data

Sample	$^{143}Nd/^{144}Nd$	$^{87}Sr/^{86}Sr$	$^{206}Pb/^{204}Pb$	$^{207}Pb/^{204}Pb$	$^{208}Pb/^{204}Pb$
DK-1 (K1)	0·512863	0·703687	19·032	15·616	38·823
DK-10 (K1)	0·512916	0·703321			
DK-19 (K1)	0·512880	0·703303			
DK-23 (K2)	0·512856	0·703484	19·018	15·615	38·816
DK-25 (K3)	0·512924	0·703065	19·113	15·552	38·728
DK-27 (K3)	0·512933	0·703095			
DK-29 (K2)	0·512881	0·703379	19·130	15·595	38·874
DK-52 (K2)	0·512878	0·703683			
DK-58 (K1a)	0·512657	0·704303	18·873	15·636	38·828
DO-59 (O1)	0·512794	0·704063	18·948	15·628	38·752
DO-62 (O2)	0·512816	0·703722	18·832	15·606	38·729
DO-64 (O3)	0·512928	0·703235			
DO-67 (O3)	0·512880	0·703501			
DO-68 (O1)	0·512864	0·703726	18·989	15·594	38·820

in $^{87}Sr/^{86}Sr$ that we have recognized is similar to that documented by Lustrino *et al.* (2012), but offset to slightly lower values. Our new data reveal a significantly larger range in $^{143}Nd/^{144}Nd$, largely owing to the small number of samples for which Lustrino *et al.* (2012) determined Nd isotopic ratios.

We have previously documented that much of the isotopic variation in the Siverek lavas can be attributed to crustal contamination (Ekici *et al.*, 2012). Our new data reveal that there are significant variations in major and trace element chemistry within both the Karacadağ and Ovabağ phases. For Mt. Karacadağ this variation also involves a spatial aspect, with K1 lavas being clustered close to the northern summit and K3 close to the central summit (Fig. 1b). Thus, before evaluating changes in the mantle sources we must determine the role of differentiation, including crustal contamination, in generating the chemical diversity of the Karacadağ and Ovabağ lavas.

Fractional crystallization

Most lavas in this study have relatively high MgO contents. The main exception to this is group K1, in which MgO varies between 2·3 and 6·7 wt %, suggesting moderate to extensive differentiation of the primary magma. Some K3 lavas also have slightly more evolved compositions, with MgO contents of ~6 wt %. To examine whether fractional crystallization could generate the variations within these groups we undertook modelling using alphaMELTS software (Smith & Asimow, 2005).

The low MgO contents of the K1 lavas suggest that none of these represent a parental magma; however, most ratios of incompatible trace elements in K1 lavas are very similar to those of group K2 (Figs 4 and 5). Therefore, we selected a primitive group K2 lava, KD-102, as the starting composition with which to attempt to replicate variations within group K1. For K3 lavas, which cannot be produced from a K2 parent, we chose KD-26, the member of this group with the most elevated MgO. Relatively low water contents (0·35 wt %) were assumed for both parent magma compositions and the oxygen fugacity was set at the quartz–fayalite–magnetite (QFM) buffer. More extreme values for either of these parameters failed to generate suitable fits to the data. Specifically, elevated fO_2 resulted in early oxide saturation whereas more elevated H_2O suppressed plagioclase crystallization in lower pressure model runs. An iterative approach revealed that only a narrow range of differentiation conditions replicated the compositional variation of each group.

Major element variations in group K1 can be replicated through fractional crystallization of KD-102 at 5 MPa. In this model the initial stages of crystallization, which account for removal of less than 10% of the original mass of the melt, are dominated by olivine with minor spinel. This stage is able to generate much of the major element variation observed in the K2 group, although there is some scatter in the alkali and alkaline earth elements (see below). Group K1 closely resemble melts generated after olivine is replaced on the liquidus by clinopyroxene at *c.* 7 wt % MgO (Fig. 7). The proportion of spinel crystallizing in the 5 MPa model increases significantly at 5 wt % MgO, which corresponds to a significant inflection in TiO_2, Fe_2O_3 and V in the K1 data array (Figs 3 and 7) although some groundmass clinopyroxene in K1 lavas is titanaugite, which could also contribute to depletion of these elements. At around 4 wt % MgO the model precipitated plagioclase. This is consistent with the very minor inflections for Al_2O_3 (Figs 2 and 7) at which point slightly less than 40% of the original melt had crystallized. The models are also consistent with petrographic observations of olivine ± clinopyroxene ± oxide ± plagioclase phenocryst assemblages in most Karacadağ phase lavas.

To explore the role of fractional crystallization further we examined the ratios of incompatible trace elements with similar bulk partition coefficients. Most group K1 and K2 lavas show no systematic variation in such ratios with changing MgO (Fig. 5). There is relatively little variation of these ratios and almost complete overlap in the ratios of groups K1 and K2 (Fig. 5). Therefore, we are confident that the model generated from the alphaMELTS software captures the important features of differentiation in these groups. However, there are two deviations from expected behaviour. First, Sm/Zr shows a systematic change within group K1 (Fig. 5f). This appears to be part of a progressive depletion in the middle REE (MREE) and HREE, relative to other elements with similar

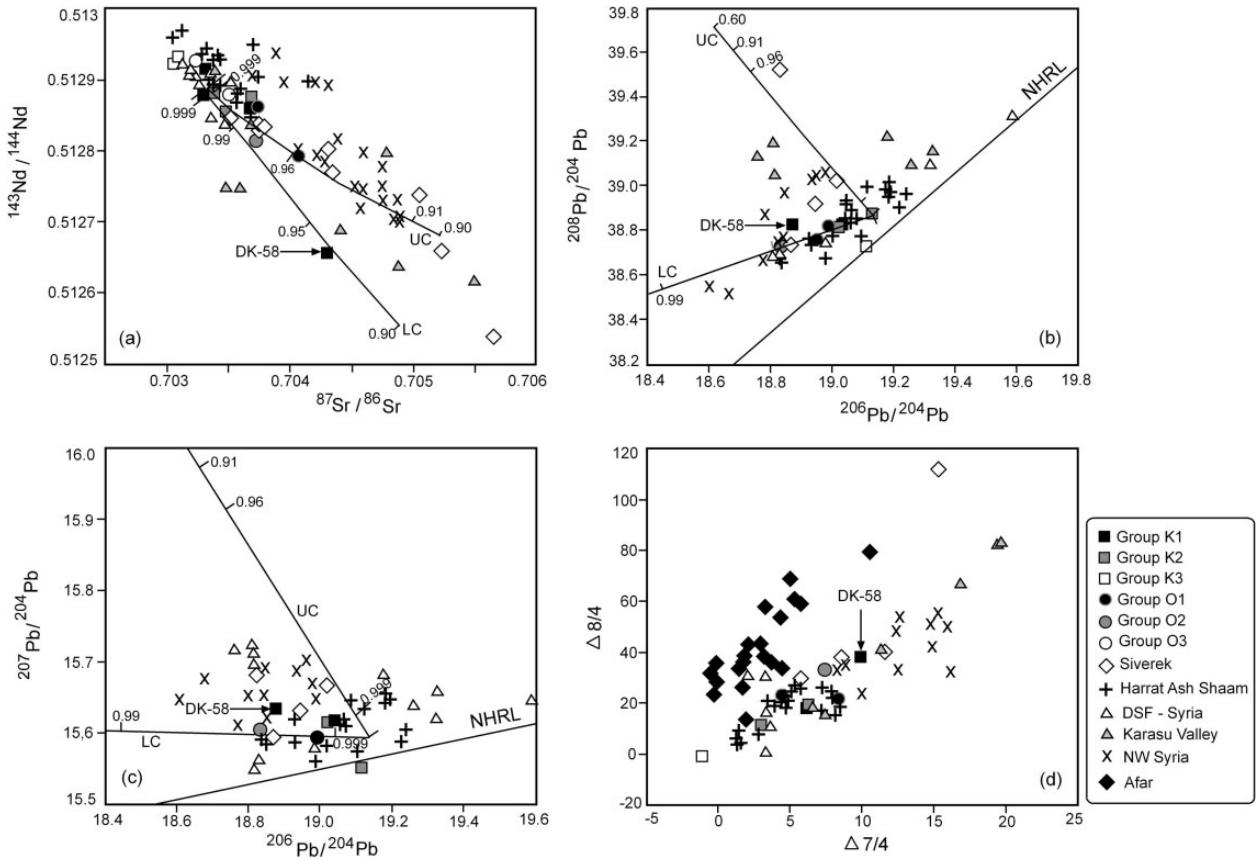

Fig. 6. (a) $^{87}Sr/^{86}Sr$ vs $^{143}Nd/^{144}Nd$, (b) $^{208}Pb/^{204}Pb$ vs $^{206}Pb/^{204}Pb$, (c) $^{207}Pb/^{204}Pb$ vs $^{206}Pb/^{204}Pb$, and (d) Δ7/4 Pb vs Δ8/4 Pb for Karacadağ and Ovabağ lavas from the Karacadağ Volcanic Complex (KVC). Other data sources: KVC Siverek plateau lavas from Lustrino *et al.* (2010) and Ekici *et al.* (2012); Karasu Valley from Çapan *et al.* (1987); NW Syria from Krienitz *et al.* (2006), Dead Sea Fault in Syria (DSF–Syria) from Ma *et al.* (2011); Harrat Ash Shaam in Jordan from Shaw *et al.* (2003); lavas that have been attributed to a plume component beneath Afar from Deniel *et al.* (1994) and Pik *et al.* (1999). The Northern Hemisphere Reference Line (NHRL) in (b) and (c) is from Hart (1984). Black curves are models of assimilation with fractional crystallization (De Paolo, 1981) for a parental magma with the composition of lava DK-29. Ticks marks on the curves represent values for melt remaining (F) of 0·999, 0·995, 0·993, 0·99 then 0·01 increments to 0·95 and 0·05 increments subsequently. UC is contamination of DK-29 by upper crust (Sr = 69 ppm, Nd = 18·5 ppm, Pb = 48 ppm, $^{87}Sr/^{86}Sr = 0{\cdot}764478$, $^{143}Nd/^{144}Nd = 0{\cdot}511398$, $^{206}Pb/^{204}Pb = 18{\cdot}598$, $^{207}Pb/^{204}Pb = 16{\cdot}026$, $^{208}Pb/^{204}Pb = 39{\cdot}746$); LC is contamination by lower crust (Sr = 814 ppm, Nd = 29·94 ppm, Pb = 30 ppm, $^{87}Sr/^{86}Sr = 0{\cdot}709028$, $^{143}Nd/^{144}Nd = 0{\cdot}511270$, $^{206}Pb/^{204}Pb = 16{\cdot}926$, $^{207}Pb/^{204}Pb = 15{\cdot}622$, $^{208}Pb/^{204}Pb = 37{\cdot}804$). Crustal compositions from Davidson & Wilson (1989).

compatibility, with decreasing MgO in K1 lavas. Because the absolute concentrations of REE increase with decreasing MgO (compare ytterbium in Fig. 2) we attribute this to the MREE and HREE behaving slightly less incompatibly than normally expected during crystallization of the magma. Second, a small subset of group K1 has elevated K/La and Ba/Yb at a particular value of MgO. Because Ba/Yb has previously been proposed as a proxy for crustal contamination in the Karacadağ Volcanic Complex we have identified this subset as Group K1a in Figs 3, 5 and 7. Their development is discussed in the next section.

Group K3 compositions cannot be generated from a K2 parent, or vice versa. Therefore, the K3 series records a distinct initial melt, and its major element variations suggest differentiation under different conditions. In particular, garnet crystallization is required to suppress Al_2O_3 enrichment (with decreasing MgO) whilst matching the other K3 major element characteristics. For the DK-26 parent composition the optimum alphaMELTS model involves differentiation at 22·5 MPa, initially of 5% orthopyroxene with minor spinel, followed by removal of an assemblage comprising garnet, clinopyroxene and spinel. This achieves the enrichment of K_2O and N_2O whilst suppressing Al_2O_3 and SiO_2 enrichment and also depleting CaO in the melt (Fig. 7).

Ovabağ phase lavas display restricted ranges in concentration of all major elements, implying that fractional crystallization played a limited role in the evolution of these magmas. As for group K2, the restricted variations within groups O1 and O2 can be replicated by removal of less than 10% olivine, with minor spinel, from a parental basalt with around 10 wt % MgO. The similarity of

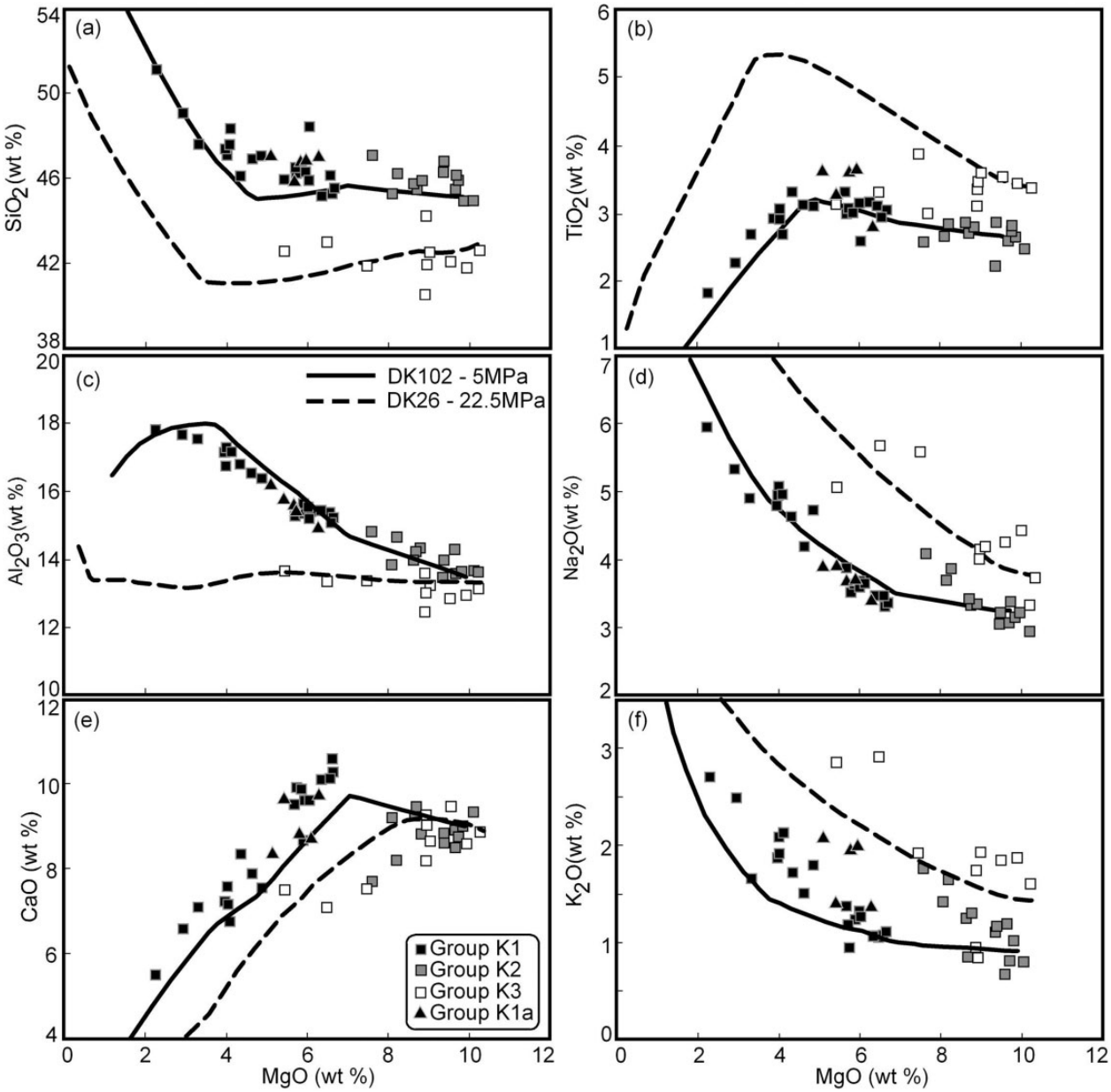

Fig. 7. Variation of selected major elements vs MgO for Karacadağ phase lavas from the Karacadağ Volcanic Complex. Fractional crystallization models generated using alphaMELTS (Smith & Asimow, 2005) for KD-l02 at 5 MPa (continuous line) and DK-26 at 22·5 MPa (dashed line). (See text for details.)

group O3 to group K3 suggests that these also differentiated at relatively high pressure.

Crustal contamination

Crustal contamination is known to have affected Neogene and Quaternary magmatism throughout the Arabian Plate (Baker *et al.*, 2000; Shaw *et al.*, 2003; Krienitz *et al.*, 2009; Ma *et al.*, 2011). For example, despite the absence of crustal xenoliths or xenocrysts in the Miocene Siverek lavas of the Karacadağ Volcanic Complex, variations towards higher $^{87}Sr/^{86}Sr$, Δ7/4Pb and Δ8/4Pb and lower $^{143}Nd/^{144}Nd$ demonstrate that some of those lavas have interacted with the crust (Ekici *et al.*, 2012). Contamination was not a ubiquitous process, however, with only some Siverek lavas having an isotopic signature indicating interaction with the crust. This contamination had a negligible impact on incompatible trace element contents and ratios, except for enriching Ba with respect to other elements. Selective Ba enrichment most probably occurred because the contamination leverage for this element—its

concentration in the contaminant relative to the magma—was significantly higher than that of other elements.

Concentrations of incompatible trace elements in the Pliocene–Quaternary lavas are similar to or greater than those in the most trace element enriched Siverek basalts. Therefore, the same set of country rocks should exert even less contamination leverage upon incompatible trace element concentrations in the Karacadağ and Ovabağ phase magmas than was the case for Siverek. This is evaluated further in Fig. 5. Rocks containing more than 8 wt % MgO display the full range for most incompatible trace element ratios and show no obvious correlations either within particular groups or in the datasets as a whole. This observation suggests that ranges for these ratios were present in the most primitive magma batches and that crustal contamination had a negligible impact upon the trace element chemistry of the most Mg-rich magmas. The highest Ba/Yb ratios occur in the two most evolved members of group K3 (Fig. 5), yet these same two samples show the lowest $^{87}Sr/^{86}Sr$, Δ7/4Pb and Δ8/4Pb, and highest $^{143}Nd/^{144}Nd$ observed for the Karacadağ and Ovabağ phases, suggesting that a crustal influence is not required to generate the range of trace element ratios observed in this magmatism.

Further insight comes from comparing the incompatible trace element ratios of groups K1 and K2, which have been shown to be related by fractional crystallization. The small subset of K1a lavas, with elevated Ba/Yb and K/La at a given value of MgO, includes sample DK-58 (Fig. 5), which has the most extreme isotopic composition of all the Pliocene–Quaternary lavas (Fig. 6). However, the changes to incompatible trace element ratios are small and not systematic for all elements. For example, although group K1a lavas all have elevated K/La and Ba/Yb (Fig. 5c), some do not show elevated K_2O or Ba at a given MgO content, relative to the rest of group K1 (Fig. 3). Similarly, there are some other group K1 lavas that have elevated K_2O and Ba but not elevated K/La and Ba/Yb. There are negligible differences of the concentrations of most major and trace elements in groups K1 and K1a. Only the alkali and alkaline earth elements show systematic, although small, enrichments in the latter (Figs 3 and 7). These apparently contradictory observations probably reflect the low contamination leverage of most crustal rocks on the trace element contents of the magmas forming the Karacadağ Volcanic Complex. Thus, although the K1a group suggests that some magma–crust interaction has occurred, the restricted magnitude of the variations suggests that most trace element and isotopic ratios in the Karacadağ and Ovabağ phase magmas were not modified significantly by crustal contamination.

Modelling the contamination that has occurred is hampered by the absence of data for suitable crustal rocks for northern Arabia, a problem that has been recognized in several studies (Shaw *et al.*, 2003; Krienitz *et al.*, 2006, 2009; Ma *et al.*, 2011). To estimate the amount of melt–crust interaction we employed the approach of Ekici *et al.* (2012), who used Sudanese lithologies to investigate crustal contamination of the Siverek plateau basalts. These offer a range of Sr, Nd and Pb isotopic compositions with which to constrain the role of crustal rocks. In taking this approach we are not trying to advocate any shared provenance between Sudanese and Turkish basement but are testing the suitability of upper versus lower crustal rocks as contaminants within the northern Arabian lithosphere. Because the K2 group is parental to group K1 we used the K2 sample with the most elevated $^{143}Nd/^{144}Nd$ (KD-29) as the primitive magma in these models.

Contamination of a magma with the initial isotopic composition of DK-29 by lower crust provides a good fit to the Nd–Sr isotopic ratios of DK-58 with only a limited amount of differentiation ($F = 0{\cdot}93$) for a relatively high ratio of assimilation to crystallization ($r = 0{\cdot}75$; model LC in Fig. 6). Contamination by upper crust does not produce such low $^{143}Nd/^{144}Nd$ relative to $^{87}Sr/^{86}Sr$ as seen in DK-58. The lower crust model also provides a more suitable fit to the displacement of DK-58 in Pb isotope space. However, the amount of contaminant required to produce the Sr and Nd isotopic variation would, in most cases, lead to substantially more extreme Pb isotopic ratios than observed in DK-58. This may be because the parental melt was significantly richer in Pb than DK-29 or that the crust beneath Karacadağ was able to exert considerably less Pb isotopic leverage than these models suggest. In either case, the amount of contamination suggested by Pb is substantially less than estimated from $^{87}Sr/^{86}Sr$ and $^{143}Nd/^{144}Nd$ for DK-58. Therefore, we consider that the Sr and Nd isotope data provide an upper limit for contamination of 5% and suggest that most batches of magma experienced substantially less contamination than this.

Composition of the mantle source

Crustal contamination has introduced little isotopic and trace element heterogeneity into the magmas of the Karacadağ and Ovabağ phases. Therefore, most of the variation in these lavas must have existed in their parental magmas. Previous studies of northern Arabian Plate volcanism have advocated peridotitic sources with elemental concentrations resembling primitive mantle (Shaw *et al.*, 2003; Ekici *et al.*, 2012). In addition, Ma *et al.* (2011) invoked garnet-bearing hornblendite veins to explain the incompatible trace element characteristics of low-silica lavas from the northern Dead Sea Fault. In this section, we shall explore the origin of the variation in the source of the Karacadağ Volcanic Complex lavas. Because group K1 experienced greater differentiation than the remaining groups we exclude these whilst constraining the trace element characteristics of mantle sources beneath the north Arabian Plate. However, we include relevant K1 data

when considering isotopic ratios to place further constraints upon those sources.

The Ovabağ data show how the rare earth element systematics of the Karacadağ Volcanic Complex lavas can be reconciled with fractional, non-modal melting of peridotite with element concentrations resembling primitive mantle, with or without a small amount of MREE enrichment (Shaw *et al.*, 2003; Ekici *et al.*, 2012). Groups O2 through O1 to O3 form a shallow, positive array in Dy/Yb vs La/Yb space (Fig. 8a). The low Dy/Yb ratios in the group O2 lavas coincide with the spinel lherzolite melting model suggesting low degrees of melting (2–3%) of a relatively shallow source. Groups O1 and O3 form a tight cluster trending from O2 values towards a restricted range of compositions with high Dy/Yb and La/Yb, which could represent low-degree (<1·5%) partial melting of a garnet lherzolite. Groups O2 and O3 could therefore represent mixtures of melt from primitive spinel lherzolite with progressively greater amounts of melt derived from below the spinel–garnet transition. The tight array suggests little variation in the degree of partial melting in the shallow and deep sources. The greater prominence of low degrees of partial melting implied for the group O3 lavas is also consistent with their higher trace element contents (Fig. 3). Groups K2 and K3 can be interpreted in a similar way but are displaced from the Ovabağ array to intersect the modelled melting curves at higher degrees of melting (Fig. 8a). In addition, the more elevated Dy/Yb values in group K3 also indicate a greater relative contribution from garnet lherzolite.

Models invoking primitive mantle concentrations of REE provide valuable information on the relative melt contributions from different depths during polybaric melting of the mantle. However, the Karacadağ Volcanic Complex lavas show fractionation of large ion lithophile elements from both the rare earth elements and high field strength elements, which cannot be produced by melts of primitive spinel and garnet lherzolite alone (Fig. 8c). These fractionations also preclude an origin involving only primitive mantle and hornblendite veins as proposed by Ma *et al.* (2011), which cannot generate the $(K/La)_n$ values greater than unity that are common to groups K2, O1 and O2. The low K/La and K/Nb ratios of group K3 lavas could be interpreted as reflecting derivation from a source containing hornblendite (Fig. 8c) but their elevated and variable Dy/Yb ratios are not consistent with this origin (Fig. 8a). Furthermore, low Sm/Zr ratios suggest a limited or non-existent role for this lithology in the genesis of all Karacadağ Volcanic Complex lavas (Fig. 8d).

Incompatible trace element ratios of Karacadağ and Ovabağ lavas are not consistent with derivation from a carbonated mantle source (Nelson *et al.*, 1988; Blundy & Dalton, 2000; Dixon *et al.*, 2008; Sisson *et al.*, 2009). They display low Ba/Th and elevated Nb/La, with the most silica-poor (Mg-rich) magma compositions having the lowest La/Nb (Fig. 5e); Zr depletion is negligible (Figs 4 and 5f). These signatures also contrast with those proposed for carbonated mantle in the northern Arabian Plate (Shaw *et al.*, 2007). Therefore, in an attempt to reproduce the incompatible trace element variation we modelled partial melting of hydrous garnet lherzolite (Fig. 9). Fractional, non-modal melting was considered for two sources. First, we explored the amphibole-bearing source and melting proportions given by Ma *et al.* (2011). The second model was a phlogopite–garnet peridotite from Sisson *et al.* (2009), using partition coefficients from Sisson *et al.* (2009) and Adam & Green (2006). Neither model, by itself, reproduces the range of compositions observed in the Karacadağ Volcanic Complex lavas or in the different groups that we have identified. However, mixtures of melts from phlogopite-bearing mantle and anhydrous sources with a small enrichment of the most incompatible elements can achieve many of the key characteristics (Sisson *et al.*, 2009).

Mixtures between melt from an amphibole–garnet lherzolite and an anhydrous, enriched (garnet or spinel) lherzolite cannot reproduce the low Ba/La and Ba/Yb and relatively high Zr/Nb ratios seen in many of the lavas from the Karacadağ and Ovabağ phases (Fig. 9a, c and d). Such a source does, however, provide a particularly good fit to Jordanian Harrat Ash Shaam lavas (Shaw *et al.*, 2007) for all ratios except Rb/Ba (see below). This suggests that the trace element enrichment of the magmatism close to the Syrian–Jordanian border may be due to the presence of significant amounts of amphibole in the mantle (Fig. 9a, c and d), whereas amphibole does not appear be an important component in the mantle beneath Karacadağ.

Although melts from phlogopite–garnet lherzolite are not suitable as sole sources they do display some of the key trace element features that characterize the Karacadağ and Ovabağ lavas. Elevated Zr/Nb at low K/La, and low Ba/Yb and Ba/La are all predicted for melts derived from this source (Fig. 9a, c and d). Because REE systematics suggests derivation over a range of depths (Fig. 8a) we suggest that the Pliocene to Quaternary Karacadağ Volcanic Complex lavas were derived from mixtures of melt derived from three sources: phlogopite-bearing garnet lherzolite, enriched garnet lherzolite and enriched spinel lherzolite. No simple binary mixtures can reproduce the entire data array. However, mixtures of 1·5–5% partial melt of phlogopite–garnet peridotite with low-degree (<1%) partial melts of anhydrous lherzolite reproduce most of the key features (Fig. 9a, c and d). The major problem comes in reproducing the low Rb/Ba ratios of the northern Arabian intra-plate magmatic suites (Fig. 9). We have tried various manipulations of the models to achieve low Rb/Ba, particularly coupled to elevated La/Yb (Fig. 9b)

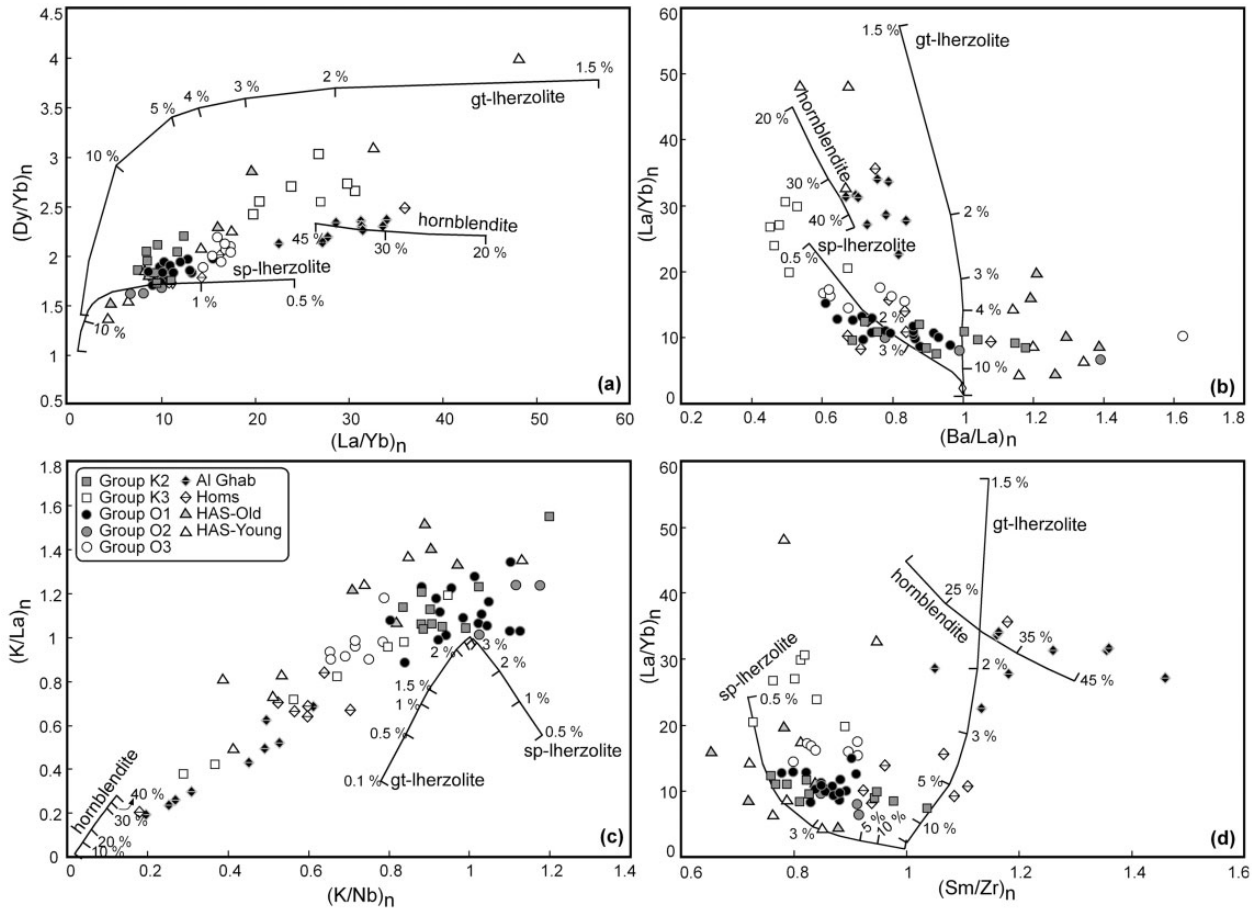

Fig. 8. (a) La/Yb vs Dy/Yb, (b) Ba/La vs La/Yb, (c) K/Nb vs K/La, and (d) Sm/Zr vs La/Yb for Pliocene to Quaternary Karacadağ Volcanic Complex lavas normalized (subscript n) to primitive mantle (McDonough & Sun, 1995). Data from Al Ghab and Homs within the Dead Sea Fault zone (Ma *et al.*, 2011) and Harrat Ash Shaam (HAS) in Jordan (Shaw *et al.*, 2003) are included for comparison. Melting models shown use partition coefficients from Adam & Green (2006), except for spinel and potassium in phases not listed in that paper, for which we the data of Ma *et al.* (2011) are used. Melting models for garnet and spinel lherzolite use the primitive mantle composition of McDonough & Sun (1995), and the modal and melting proportions of Thirlwall *et a.* (1994). For hornblendite, the initial composition and melting proportions are from Ma *et al.* (2011). Tick marks indicate total melt fraction.

whilst maintaining the fits achieved for other ratios. We speculate that the most likely solution is a relatively high partition coefficient for Rb in phlogopite (e.g. $D_{\mathrm{Rb}}^{\mathrm{phlog}} > 8$), which is not unreasonable (Ionov *et al.*, 1997).

Thus, we propose that most Karacadağ Volcanic Complex lavas originated as mixtures of (1) melt derived from enriched, anhydrous lherzolite over a range of depths, with (2) melt derived from phlogopite-bearing garnet lherzolite. Whereas lavas from Harrat Ash Shaam or the northern Dead Sea Fault appear to record evidence for amphibole in their sources (Shaw *et al.*, 2003; Ma *et al.*, 2011) there is little evidence to support its involvement at Karacadağ (Figs 8 and 9). Having invoked multi-component mixing in the mantle it is difficult to place quantitative constraints on the degree of partial melting. However, using the REE, which should be modified by metasomatism in a relatively systematic fashion, suggests that the Pliocene to Quaternary Karacadağ Volcanic Complex lavas formed through small degrees of partial melting similar to those calculated for other parts of the northern Arabian Plate (Fig. 7a).

Origin of the mantle sources

Previous studies have identified a number of potential mantle sources beneath the Arabian Plate that could contribute to intraplate magmatism. These include lithospheric mantle, variably enriched by metasomatism, the convecting upper mantle and outflow of mantle from the Afar triple junction (Çapan *et al.*, 1987; Pearce *et al.*, 1990; Camp & Roobol, 1992; Bertrand *et al.*, 2003; Shaw *et al.*, 2003; Şen *et al.*, 2004; Weinstein *et al.*, 2006; Krienitz *et al.*, 2006, 2007, 2009; Lustrino *et al.*, 2010; Ma *et al.*, 2011; Ekici *et al.*, 2012). Most of these studies have identified multiple source components at any one site. In this section we

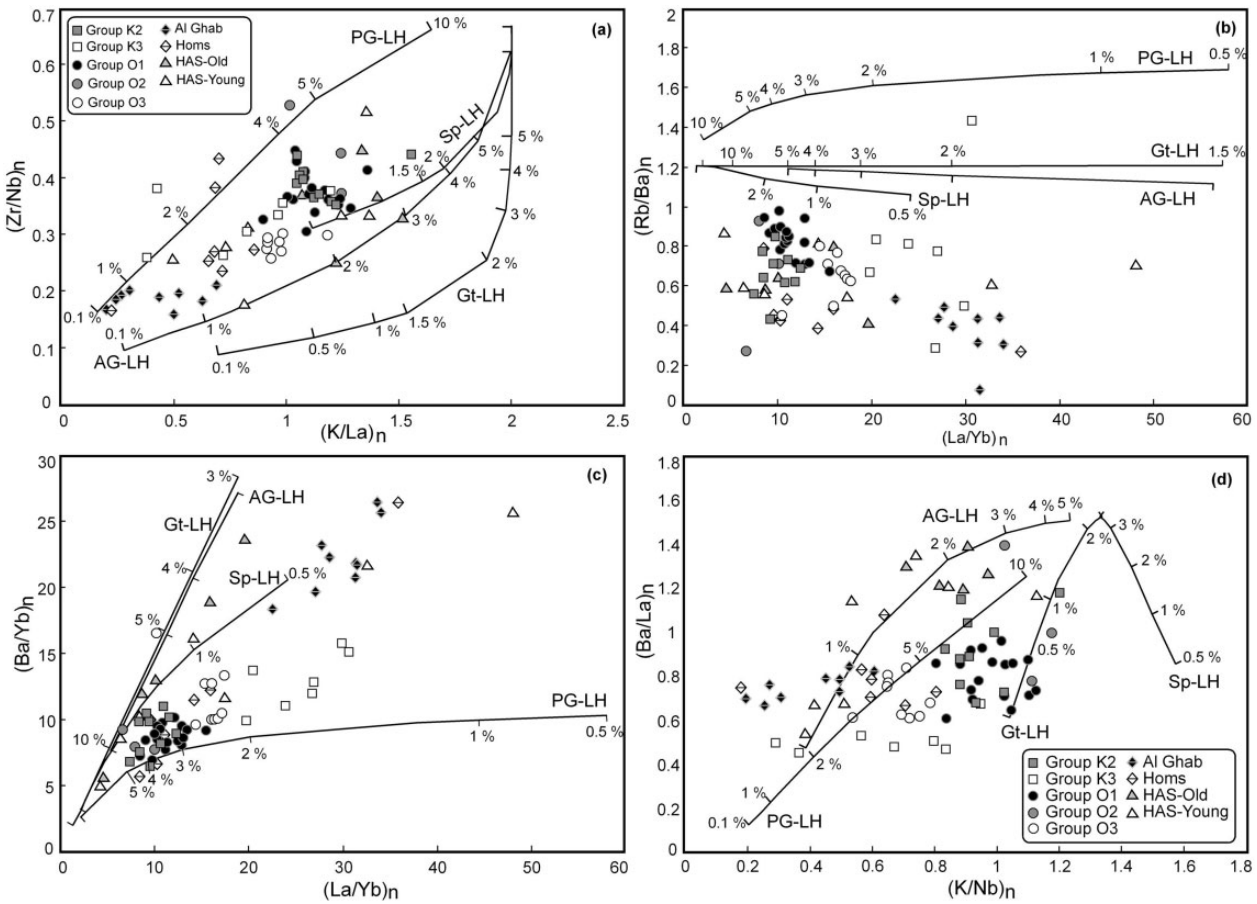

Fig. 9. (a) K/La vs Zr/Nb, (b) La/Yb vs Rb/Ba, (c) La/Yb vs Ba/Yb, and (d) K/Nb vs Ba/La for Pliocene to Quaternary Karacadağ Volcanic Complex lavas normalized to primitive mantle (McDonough & Sun, 1995). (For sources of data from other volcanic fields see caption to Fig. 6.) Melting models use abundances in primitive mantle. Garnet lherzolite (Gt-LH) and spinel lherzolite (Sp-LH) models are as described in the caption to Fig. 6, except that large ion lithophile elements were increased by a factor of two (Sisson *et al.*, 2009). Modal and melting proportions are from Ma *et al.* (2011) for amphibole–garnet lherzolite (AG-LH) and from Sisson *et al.* (2009) for phlogopite–garnet lherzolite (PG-LH). Tick marks indicate total melt fractions.

compare the isotopic compositions of Pliocene to Quaternary magmatism in the Karacadağ Volcanic Complex with other locations in the northern Arabian Plate and discuss the implications for mantle sources throughout this area.

Karacadağ Volcanic Complex lavas lack $^{206}Pb/^{204}Pb$ in excess of 19·1, in contrast to those from the Harrat Ash Shaam, Dead Sea Fault and northern Syria, where a high $^{206}Pb/^{204}Pb$ component has been identified (Bertrand *et al.*, 2003; Krienitz *et al.*, 2009; Ma *et al.*, 2011). This component is most conspicuous in high $^{206}Pb/^{204}Pb$ lavas from Karasu Valley and the Dead Sea Fault, from which a $^{206}Pb/^{204}Pb$ ratio greater than 19·5, with $^{207}Pb/^{204}Pb$ and $^{208}Pb/^{204}Pb$ close to the Northern Hemisphere Reference Line, can be inferred (Fig. 6c and d). This high $^{206}Pb/^{204}Pb$ component was attributed to the Afar plume by Krienitz *et al.* (2009), although others have suggested that it represents an older, lithospheric source (Bertrand *et al.*, 2003). A clear distinction between the Δ8/4Pb values of Afar plume magmatism and Arabian intraplate lavas, including the Karacadağ Volcanic Complex, precludes involvement of the Afar plume in the magmatism of the northernmost Arabian Plate (Fig. 6d). Regardless of its origin, however, the high $^{206}Pb/^{204}Pb$ component has not made a significant contribution to Karacadağ Volcanic Complex magmatism.

A group K3 lava has the lowest $^{207}Pb/^{204}Pb$ and $^{208}Pb/^{204}Pb$ for a given $^{206}Pb/^{204}Pb$ of any sample from the Karacadağ Volcanic Complex. The Sr and Nd isotopic composition of this sample (DK-25) is similar to those of low $^{206}Pb/^{204}Pb$ samples from Harrat Ash Shaam and northern Syria (Bertrand *et al.*, 2003; Shaw *et al.*, 2003; Krienitz *et al.*, 2009). Therefore, we interpret this as an end-member that is common to much of the intraplate magmatism across northern Arabia and, as previously suggested by Shaw *et al.* (2003) and Krienitz *et al.* (2009), the

low $^{206}Pb/^{204}Pb$, Δ7/4Pb, Δ8/4Pb and $^{87}Sr/^{86}Sr$ and high $^{143}Nd/^{144}Nd$ indicate that this is probably depleted upper mantle. Rare earth element systematics demonstrate that group K3 lavas contain a relatively large contribution from the garnet stability field and so the distinctive K3 isotopic composition could reflect melt derived from either lithospheric or asthenospheric mantle. Workman & Hart (2005) have characterized the range of isotopic compositions in the depleted mantle as a spectrum spanning enriched (E-DMM) to depleted (D-DMM) endmembers. The isotopic ratios of DK-25 are very similar to those of E-DMM, which is likely to represent the most fusible component of the convecting mantle. Therefore, the K3 composition might represent small-degree melts from the convecting mantle, in which phlogopite can be stable (Luth, 2003). Alternatively, such melts may metasomatize the base of the lithospheric mantle (McKenzie, 1989), providing a hydrated lherzolite source resembling E-DMM that could contribute to magmatism throughout the region. Kovács *et al.* (2012) suggested that phlogopite would be the primary hydrous phase in peridotite at pressures greater than 3 GPa, although the presence of this and alternative water-bearing phases at lower pressures, principally the amphibole pargasite, is also dependent on the bulk composition and the absolute water content of the mantle.

Incompatible element systematics indicate that group K1 and K2 lavas contain greater contributions from shallower mantle (Figs 8 and 9). Melting at shallow levels could occur if asthenosphere upwells sufficiently to melt to higher degrees, so allowing increased dilution of the E-DMM component by melts from more refractory parts of the mantle (Elliott *et al.*, 1991). However, this is not consistent with the higher $^{87}Sr/^{86}Sr$ and lower $^{143}Nd/^{144}Nd$ of the group K1 and K2 lavas (Fig. 6). In addition, large degrees of asthenospheric upwelling would be difficult to reconcile with limited or highly localized extensional tectonics during magmatism at Mt. Karacadağ (Adiyaman & Chorowicz, 2002). Therefore, we suggest that the lavas of groups K1 and K2 are dominated by melts derived from enriched parts of the shallow lithospheric mantle. The enriched, lithospheric source has $^{87}Sr/^{86}Sr \sim 0{\cdot}70370$ and $^{143}Nd/^{144}Nd \sim 0{\cdot}51286$. Pb isotope ratios are more difficult to constrain owing to the possible influence of crustal contamination. However, the enriched lithosphere is likely to have slightly lower $^{206}Pb/^{204}Pb$ than the depleted component and slightly more elevated Δ7/4Pb and Δ8/4Pb (Fig. 6).

Shaw *et al.* (2003) concluded that the Jordanian part of the Harrat Ash Shaam was also derived from mixtures of deep, depleted and shallow, enriched mantle. Despite the evidence for differences in the nature of mantle hydrous phases between Karacadağ and Harrat Ash Shaam (Fig. 9), the isotopic data indicate that the two volcanic regions are probably derived from similar types of mantle.

Magma transport through the crust at Mt. Karacadağ

The thickness of single lava flows was not measured as part of this study so we cannot quantify the relative volumes of magma generated by different parts of the Karacadağ volcano. However, most lavas initially flowed laterally from the loci of eruption therefore some constraints can be obtained by observing where each group predominates along the ridge crest. We combine this information with constraints obtained from fractional crystallization models to interpret magma transport during the Karacadağ phase of magmatism. Group K1 lavas were mainly erupted on and around the northern summit of Mt. Karacadağ, but are much less abundant on the central and southern summits (Fig. 1b). Lavas of group K2, in contrast, are present along the length of the ridge. This suggests that the magmatic plumbing at the northern end of the volcano was conducive to eruption of magma that had differentiated more extensively.

Late Cenozoic stress in the northern Arabian Plate was produced by its collision with Anatolia. The resultant westward escape of Anatolia, accommodated in southern Turkey along the East Anatolian Fault (Fig. 1a), has caused different types of strain throughout northern Arabia. Adıyaman & Chorowicz (2002) attributed the Mt Karacadağ fissure to far-field, east–west tension that diminished towards the south, distal to the collision. If this tensional stress diminished southward along the Karacadağ fissure then the northern part of the volcano could have provided a larger accommodation volume in the crust into which more magma could be emplaced. This, in turn, would supply more heat into the surrounding crustal rocks, which would account for the northern K1 group providing the few examples in which we observed evidence for crustal contamination. A differentiation pressure of 5 MPa, as determined for groups K1 and K2 from the alphaMELTS models, indicates crystallization close to the postulated upper to lower crust transition of 19 km (Nasir & Safarjalani, 2000). This depth has also been proposed as the transition from brittle to ductile behaviour of the crust in northern Arabia (Adıyaman & Chorowicz, 2002). Thus, we suggest that differentiation could proceed further at the northern end of Mt. Karacadağ as a result of relatively large volumes of magma ponding close to the petrological and rheological boundary between upper and lower crust (Fig. 10). Elsewhere along the fissure, the cooler crust would have impeded development of extensive magma storage zones and the magmas experienced less differentiation, resulting in the more primitive K2 lava flows.

Group K3 has a restricted distribution on the Mt. Karacadağ ridge, being the predominant lava type of the central summit with a minor presence on the northern summit (Fig. 1b). Most of these lavas have elevated MgO

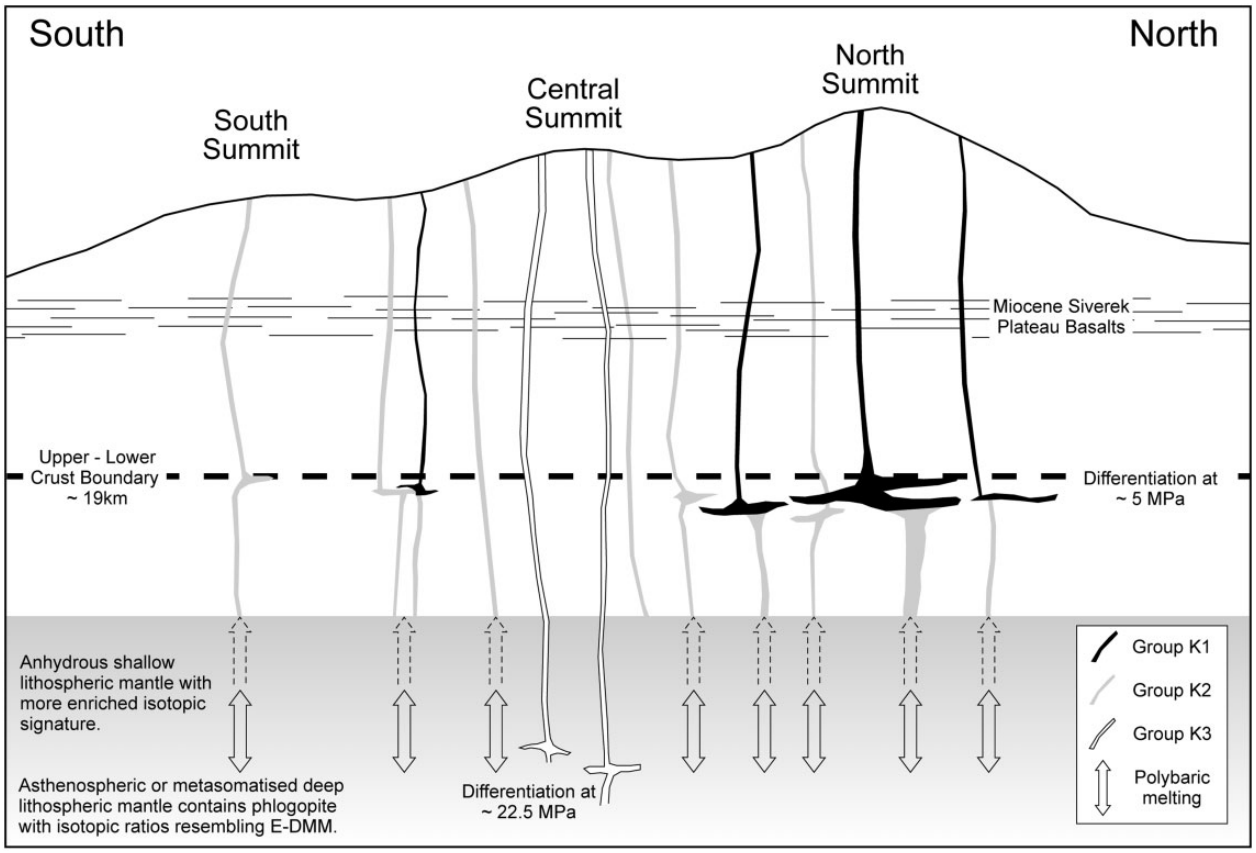

Fig. 10. Sketch section illustrating the petrogenesis of the Mt Karacadağ magmas. Siverek plateau basalts were erupted during the Miocene and form the substrate onto which the Karacadağ lavas were erupted. The vertical axis is schematic and is not to scale. Constraints on the depth of the upper–lower crust boundary come from geophysical data and xenolith petrology (see text for details). Differentiation depths are from alphaMELTS models. Group K1 and K2 lavas share similar sources that represent polybaric melting but with a relatively large contribution from the spinel stability field, whereas group K3 lavas contain a larger contribution from deeper, garnet-bearing mantle. Group K2 lavas have experienced relatively restricted amounts of differentiation close to the upper–lower crust boundary and are found along the length of the volcano. Lavas of group K1 occur predominantly in the north and developed when group K2 magma experienced more extensive differentiation at the upper–lower crustal transition. Group K3 lavas experienced small amounts of differentiation close to the base of the lithosphere.

contents and the fractional crystallization models reflect very restricted amounts of differentiation. The distinctive chemistry of this group, however, does require differentiation at high pressure (Fig. 7) and it is tempting to equate the modelled pressure of 22·5 MPa with the 80 km depth estimated for the lithosphere–asthenosphere transition zone in northern Arabia (McGuire & Bohannon, 1989; Nasir & Safarjalani, 2000). The lack of evidence for low-pressure crystallization suggests that, subsequent to fractionation close to the base of the lithosphere, group K3 magmas experienced negligible further differentiation before eruption.

CONCLUSIONS

Mt. Karacadağ is the most conspicuous feature of the Karacadağ Volcanic Complex, forming an elongate shield volcano that has produced lateral lava flows from its north–south-oriented axis. This form suggests that lithospheric tension localized magmatism during Pliocene and Quaternary times. East–west tension in this part of the Arabian Plate was the result of local stress caused by the initiation of the Eastern Anatolian Fault (Adıyaman & Chorowicz, 2002). Late in the history of the Karacadağ Volcanic Complex magmatism migrated to Ovabağ, where lavas were erupted from monogenetic cones and represent melting and magma emplacement in the absence of significant lithospheric tension.

Previously, we interpreted the earlier, Miocene phase of magmatism as the result of melting when mantle upwelled beneath a lithospheric weak spot as the Arabian Plate migrated north and east during the Cenozoic (Ekici *et al.*, 2012). The Karacadağ and Ovabağ phases may represent renewed melting through this process although localized tectonic processes served to focus magmatism. In the case of Mt. Karacadağ, localized extension may also have played a role in causing melting, but there is restricted geological evidence at the surface to support this. Isotopic

data indicate that mantle derived from the Afar plume was not involved in genesis of Karacadağ Volcanic Complex lavas.

Trace element systematics of the Karacadağ Volcanic Complex lavas were influenced by the presence or absence of small quantities (<2%) of phlogopite in the mantle. The lavas do not display evidence for derivation exclusively from amphibole veins in the mantle as proposed for the magmatism of the Al Ghab volcanic field within the Dead Sea Fault zone (Ma *et al.*, 2011) or for melting of carbonated mantle (Shaw *et al.*, 2007).

The group K3 and O3 lavas are distinct in their low contents of silica and Al_2O_3 and their elevated TiO_2 and incompatible element contents relative to other groups. Depletion in potassium, relative to other elements of similar compatibilities, coupled with the absence of extreme Ba enrichment suggests that phlogopite was present in the source of these lavas. These groups display trace element ratios that indicate a relatively large contribution from garnet-facies lherzolite. The isotopic characteristics of the lavas resemble the most fusible part of the convecting upper mantle but such a signature could also be transferred to the base of the lithospheric mantle by migration of low-degree melts. This component is common to other volcanic fields across northern Arabia. Once generated, K3 and O3 magmas experienced minor differentiation near the base of the lithosphere prior to eruption.

Groups K2, O1 and O2 represent melting across a range of depths but with a greater contribution from spinel lherzolite in the lithospheric mantle than in the K3 and O3 groups. These groups also have more elevated $^{87}Sr/^{86}Sr$ and Pb isotopic ratios and lower $^{143}Nd/^{144}Nd$ than groups K3 and O3. Group K2 magmas were produced along the length of the 30 km Karacadağ fissure and crystallized limited amounts of olivine close to the transition between upper and lower crust. At the northern end of the Mt. Karacadağ volcano more protracted differentiation of K2 parental magma at the upper–lower crust transition produced the magmas of group K1. This and the greater amount of crustal contamination observed to the north resulted from greater stress in the crust at the Anatolian end of the Karacadağ fissure. Lavas from groups O1 and O2 show similar trace element and isotopic systematics to Group K2, suggesting that mantle sources sampled by the Karacadağ phase could be generated in the absence of significant lithospheric extension.

ACKNOWLEDGEMENTS

Colin Macpherson is grateful to Durham University for a period of research leave. We thank Mark Allen and Iain Neill for discussion. Comments by Christoph Beier and an anonymous reviewer were very constructive, and led to significant improvements in this paper, as was the editorial input from Richard Price.

FUNDING

Taner Ekici acknowledges financial support from TUBITAK (Project No. 107Y025) to conduct fieldwork and analytical work. Mehmet Ülkü of MTA Diyarbakır supported fieldwork in SE Turkey.

SUPPLEMENTARY DATA

Supplementary data for this paper are available at *Journal of Petrology* online.

REFERENCES

Adam, J. & Green, T. (2006). Trace element partitioning between mica- and amphibole-bearing garnet lherzolite and anhydrous basanitic melt: 2. Tasmanian Cainozoic basalts and the origins of intraplate basaltic magmas. *Contributions to Mineralogy and Petrology* **161**, 883–899.

Adıyaman, Ö. & Chorowicz, J. (2002). Late Cenozoic tectonics and volcanism in the northwestern corner of the Arabian plate: a consequence of the strike-slip Dead Sea fault zone and the lateral escape of Anatolia. *Journal of Volcanology and Geothermal Research* **117**, 327–345.

Allen, M., Jackson, J. & Walker, R. (2004). Late Cenozoic reorganization of the Arabia–Eurasia collision and the comparison of short-term and long term deformation rates. *Tectonics* **23**, TC2008.

Baker, J. A., Macpherson, C. G., Menzies, M. A., Thirlwall, M. F., Al-Kadasi, M. & Mattey, D. P. (2000). Resolving crustal and mantle contributions to continental flood volcanism, Yemen: Constraints from mineral oxygen isotope data. *Journal of Petrology* **41**, 1805–1820.

Bertrand, H., Chazot, G., Blichert-Toft, J. & Thoral, S. (2003). Implications of widespread high-μ volcanism on the Arabian Plate for Afar mantle plume and lithosphere composition. *Chemical Geology* **198**, 47–61.

Blundy, J. & Dalton, J. (2000). Experimental comparison of trace element partitioning between clinopyroxene and melt in carbonate and silicate systems, and implications for mantle metasomatism. *Contributions to Mineralogy and Petrology* **139**, 356–371.

Brigland, D., Demir, T., Seyrek, A., Pringle, M., Westaway, R., Beck, A., Yurtmen, S. & Rowbotham, G. (2007). Dating Quaternary volcanism and incision by the River Tigris at Diyarbakır, SE Turkey. *Journal of Quaternary Science* **21**, 437–455.

Camp, V. E. & Roobol, M. J. (1992). Upwelling asthenosphere beneath western Arabia and its regional implications. *Journal of Geophysical Research* **97**, 15255–15271.

Çapan, U. Z., Vidal, P. & Contagrel, L. M. (1987). K–Ar, Nd, Sr and Pb isotopic study of Quaternary volcanism in Karasu Valley (Hatay), N end of Dead Sea rift zone in SE Turkey. *Yerbilimleri* **14**, 165–178.

Chiaradia, M., Müntener, O. & Beate, B. (2011). Enriched basaltic andesites from mid-crustal fractional crystallization, recharge, and assimilation (Pilavo volcano, Western Cordillera of Ecuador). *Journal of Petrology* **52**, 1107–1141.

Davidson, J. P. & Wilson, I. R. (1989). Evolution of an alkali basalt–trachyte suite from Jebel Marra volcano, Sudan, through assimilation and fractional crystallisation. *Earth and Planetary Science Letters* **95**, 141–160.

Demir, T., Westaway, R., Brigland, D., Pringle, M., Yurtmen, S., Beck, A. & Rowbotham, G. (2007). Ar–Ar dating of late Cenozoic basaltic volcanism in northern Syria: Implications for the history

of incision by the River Euphrates and uplift of the northern Arabian Platform. *Tectonics* **26**, TC3012.

Deniel, C., Vidal, P., Coulon, C., Vellutini, P. J. & Piquet, P. (1994). Temporal evolution of mantle sources during continental rifting: the volcanism of Djibouti (Afar). *Journal of Geophysical Research* **99**, 2853–2869.

DePaolo, D. J. (1981). Trace element and isotopic effects of combined wallrock assimilation and fractional crystallisation. *Earth and Planetary Science Letters* **53**, 189–202.

Dixon, J. E., Clague, D. A., Cousens, B., Monsalve, M. L. & Uhl, J. (2008). Carbonatite and silicate melt metasomatism of the mantle surrounding the Hawaiian plume: evidence from volatiles, trace elements, and radiogenic isotopes. *Geochemistry, Geophysics, Geosystems* **9**, Q09005.

Dungan, M. A. & Rhodes, M. J. (1978). Residual glasses and melt inclusions in basalts from DSDP legs 45 and 46: evidence for magma mixing. *Contributions to Mineralogy and Petrology* **67**, 417–431.

Ekici, T., Macpherson, C. G. & Otlu, N. (2012). Polybaric melting of a single mantle source during the Neogene Siverek phase of the Karacadağ Volcanic Complex, SE Turkey. *Lithos* **146–147**, 152–163.

Ekici, T., Macpherson, C. G. & Otlu, N. (2014). Intraplate magmatism generated by shear-induced melting during Arabian plate motion: Evidence from Volcanic Complex, southeast Turkey. *Journal of the Geological Society of London* (in press).

El-Isa, Z., Mechie, J. & Prodehl, C. (1987*a*). Shear velocity structure of Jordan from explosion seismic data. *Geophysical Journal of the Royal Astronomical Society* **90**, 265–281.

El-Isa, Z., Mechie, J., Prodehl, C., Makris, J. & Rihm, R. (1987*b*). A crustal structure study of Jordan derived from seismic refraction data. *Tectonophysics* **138**, 235–253.

Elliott, T. R., Hawkesworth, C. J. & Gronvold, K. (1991). Dynamic melting of the Iceland plume. *Nature* **351**, 201–206.

Ercan, T., Fujitani, T., Matsuda, J. I., Notsu, K., Tokel, S. & ve UI, T. (1990). Doğu ve Güneydoğu Anadolu Neojen-Kuvaterner Volkanitlerine ilişkin yeni jeokimyasal, radyometrik ve izotopik verilerin yorumu. *MTA Dergisi* **110**, 143–164.

Gürsoy, H., Tatar, O., Piper, J. D. A., Koçbulut, F. & Mesci, B. L. (2009). Paleomagnetic study of Tertiary volcanic domains in Southern Turkey and Neogene anticlockwise rotation of the Arabian Plate. *Tectonophysics* **465**, 114–127.

Hart, S. R. (1984). A large-scale isotope anomaly in the Southern Hemisphere mantle. *Nature* **309**, 753–757.

Ilani, S., Harlavan, Y., Tarawneh, K., Rabba, I., Weinberger, R., Ibrahim, K., Peltz, S. & Steinitz, G. (2001). New K–Ar ages of basalts from the Harrat Ash Shaam volcanic field in Jordan: Implications for the span and duration of the upper-mantle upwelling beneath the western Arabian plate. *Geology* **29**, 171–174.

Ionov, D. A., Griffin, W. L. & O'Reilly, S. Y. (1997). Volatile-bearing minerals and lithophile elements in the upper mantle. *Chemical Geology* **141**, 153–184.

Keskin, M. (2003). Magma generation by slab steepening and breakoff beneath a subduction–accretion complex: An alternative model for collision-related volcanism in Eastern Anatolia, Turkey. *Geophysical Research Letters* **30**, 8046.

Kovács, I., Green, D. H., Rosenthal, A., Hermann, J., O'Neil, H. S., Hibberson, W. O. & Udvardi, B. (2012). An experimental study of water in nominally anhydrous minerals in the upper mantle near the water-saturated solidus. *Journal of Petrology* **53**, 2067–2093.

Krienitz, M. S., Haase, K. M., Mezger, K., Eckardt, V. & Shaikh-Mashail, M. A. (2006). Magma genesis and crustal contamination of continental intraplate lavas in Northwestern Syria. *Contributions to Mineralogy and Petrology* **151**, 698–716.

Krienitz, M. S., Haase, K. M., Mezger, K. & Shaikh-Mashail, M. A. (2007). Magma genesis and mantle dynamics at Harrat Ash Shamah volcanic field (Southern Syria). *Journal of Petrology* **48**, 1513–1542.

Krienitz, M. S., Haase, K. M., Mezger, K., Van den Bogard, P., Thiemann, V. & Shaikh-Mashail, M. A. (2009). Tectonics events, continental intraplate volcanism, and mantle plume activity in northern Arabia: Constraints from geochemistry and Ar–Ar dating of Syrian lavas. *Geochemistry, Geophysics, Geosystems* **10**, Q04008.

Lustrino, M., Keskin, M., Mattioli, M., Lebedev, V. A., Chugaev, A., Sharkov, E. & Kavak, O. (2010). Early activity of the largest Cenozoic shield volcano in the circum-Mediterranean area: Mt. Karacadağ, SE Turkey. *European Journal of Mineralogy* **22**, 343–362.

Lustrino, M., Keskin, M., Mattioli, M. & Kavan, O. (2012). Heterogeneous mantle sources feeding the volcanic activity of Mt. Karacadağ. *Journal of Asian Earth Sciences* **46**, 120–139.

Luth, R. W. (2003). Mantle volatiles—distribution and consequences. In: Carlson, R. W. (ed.) *The Mantle and Core. Treatise on Geochemistry, Vol. 2.* Elsevier–Pergamon, pp. 319–361.

Ma, G. S.-K., Malpas, J., Xenophontos, C. & Chan, G. H.-N. (2011). Petrogenesis of latest Miocene–Quaternary continental intraplate volcanism along the northern Dead Sea Fault system (Al Ghab–Homs volcanic field), western Syria: Evidence for lithosphere–asthenosphere interaction. *Journal of Petrology* **52**, 401–430.

McDonough, W. F. & Sun, S. S. (1995). The composition of the Earth. *Chemical Geology* **120**, 223–253.

McGuire, A. V. & Bohannon, R. G. (1989). Timing of mantle upwelling: Evidence for a passive origin for the Red Sea Rift. *Journal of Geophysical Research* **94**, 1677–1682.

McKenzie, D. (1989). Some remarks on the movement of small melt fractions in the mantle. *Earth and Planetary Science Letters* **95**, 53–72.

Nasir, S. (1992). The lithosphere beneath the northwestern part of the Arabian plate (Jordan): evidence from xenoliths and geophysics. *Tectonophysics* **201**, 357–370.

Nasir, S. & Safarjalani, A. (2000). Lithospheric petrology beneath the northern part of the Arabian Plate in Syria: evidence from xenoliths in alkali basalts. *Journal of African Earth Sciences* **30**, 149–168.

Nelson, D. R., Chivas, A. R., Chappell, B. W. & McCulloch, M. T. (1988). Geochemical and isotopic systematics in carbonatites and implications for the evolution of ocean-island sources. *Geochimica et Cosmochimica Acta* **52**, 1–17.

Nelson, S. T. & Montana, A. (1992). Sieve-textured plagioclase in volcanic rocks produced by rapid decompression. *American Mineralogist* **77**, 1242–1249.

Pearce, J. A., Bender, J. F., DeLong, S. E., Kidd, W. S. F., Low, P. J., Güner, Y., Şaroğlu, F., Yılmaz, Y., Moorbath, S. & Mitchell, J. G. (1990). Genesis of collision volcanism in eastern Anatolia, Turkey. *Journal of Volcanology and Geothermal Research* **44**, 184–229.

Pik, R., Deniel, C., Coulon, C., Yirgu, G. & Marty, B. (1999). Isotopic and trace element signatures of Ethiopian flood basalts: evidence for plume–lithosphere interactions from Na/Ti and rare earth element ratios. *Journal of Geophysical Research* **104**, 2817–2829.

Robertson, A. H. F. (2000). Mesozoic–Tertiary tectonic–sedimentary evolution of a south Tethyan oceanic basin and its margins in southern Turkey. In: Bozkurt, E., Winchester, J. A. & Piper, J. D. A. (eds) *Tectonics and Magmatism in Turkey and the Surrounding Area. Geological Society, London, Special Publications* **173**, 97–138.

Şen, P. A., Temel, A. & Gourgaud, A. (2004). Petrogenetic modelling of Quaternary post-collisional volcanism: A case study of central and eastern Anatolia. *Geological Magazine* **141**, 81–98.

Şengör, A. M. C., Özeren, M. S., Keskin, M., Sakınç, M., Özbakır, A. D. & Kayan, İ. (2008). Eastern Turkish high plateau as a small

Turkish-type orogen: Implications for post-collisional crust forming processes in Turkish-type orogens. *Earth-Science Reviews* **90**, 1–48.

Shaw, J. E., Baker, J. A., Menzies, M. A., Thirlwall, M. F. & Ibrahim, K. M. (2003). Petrogenesis of the largest intraplate volcanic field on the Arabian Plate (Jordan): a mixed lithosphere–asthenosphere source activated by lithospheric extension. *Journal of Petrology* **44**, 1657–1679.

Shaw, J. E., Baker, J. A., Kent, A. J. R., Ibrahim, K. M. & Menzies, M. A. (2007). The geochemistry of the Arabian lithospheric mantle—a source for intraplate volcanism? *Journal of Petrology* **48**, 1495–1512.

Sisson, T. W., Kimura, J.-I. & Coombs, M. L. (2009). Basanite–nephelinite suite from early Kilauea: carbonated melts of phlogopite–garnet peridotite at Hawaii's leading magmatic edge. *Contributions to Mineralogy and Petrology* **158**, 803–829.

Smith, P. M. & Asimow, P. D. (2005). Adiabat_1ph: A new public front-end to the MELTS, pMELTS, and pHMELTS models. *Geochemistry, Geophysics, Geosystems* **6**, Q02004.

Thirlwall, M. F., Upton, B. G. J. & Jenkins, C. (1994). Interaction between continental lithosphere and the Iceland plume—Sr–Nd–Pb isotope geochemistry of Tertiary basalts, NE Greenland. *Journal of Petrology* **35**, 839–879.

Thy, P., Lesher, C. E. & Tegner, C. (2013). Further work on experimental plagioclase equilibria and the Skaergaard liquidus temperature. *American Mineralogist* **98**, 1360–1367.

Todt, W., Cliff, R. A., Hanser, A. & Hoffmann, A. W. (1984). $^{202}Pb + {}^{205}Pb$ double spike for lead isotopic analyses. *Terra Cognita* **4**, 209.

Weinstein, Y., Navon, O., Altherr, R. & Stein, M. (2006). The role of lithospheric mantle heterogeneity in the generation of Plio-Pleistocene alkali basaltic suites from NW Harrat Ash Shaam (Israel). *Journal of Petrology* **47**, 1017–1050.

Workman, R. K. & Hart, S. R. (2005). Major and trace element composition of the depleted MORB mantle (DMM). *Earth and Planetary Science Letters* **231**, 53–72.